Core polarization and the dielectric response of simple metals

K. Sturm
Institut für Festkörperforschung, Forschungszentrum Jülich G.m.b.H., D-5170 Jülich, West Germany

E. Zaremba
Department of Physics, Queen's University, Kingston, Ontario, Canada K7L 3N6

K. Nuroh
Department of Mathematics and Physics, Nipissing University College, North Bay, Ontario, Canada P1B 8L7
(Received 12 March 1990)

The effect of core polarization on the dielectric properties of simple metals with free-electron-like conduction bands is investigated within the random-phase approximation. The charge fluctuations of both the core and valence electrons are treated on an equal footing. The screening fields due to the core dipole moments contribute a term to the frequency-dependent dielectric function of the Clausius-Mossotti form. An important aspect of the present approach is the precise definition of the core polarizability, which is characteristic of an ion imbedded in a metal. The use of the dielectric function in a determination of the plasma frequency is found to yield excellent results in the case of Cd, In, and Sn. Results for the optical conductivity and electron-energy-loss function are also found to be in qualitative agreement with experiment for a variety of metals. Discrepancies in the plasma frequency of Al suggest that a more detailed treatment of band-structure effects may be required to obtain quantitative agreement with experiment for some metals.

I. INTRODUCTION

The dielectric response of polyvalent simple metals exhibits different behavior in the various frequency regimes of interest. In the low-frequency regime where ω is of the order of a typical energy band gap, the response properties are strongly influenced by the band structure, leading to characteristic features in the optical absorption, reflectivity, and electron-energy-loss spectrum. At higher frequencies, which can be referred to as the plasmon regime, the long-range Coulomb fields dominate the collective response of the metal; band structure is of secondary importance, and its effect can be accounted for by perturbation theory. Finally, at still higher frequencies the dynamic response of core electrons becomes important. This full range of behavior is in principle represented by the nonlocal dielectric function of the metal.

The polarization of core electrons is of course the main screening mechanism in insulators, which to a good approximation can be viewed as a collection of independent polarizable units. In metals, on the other hand, the core-electron binding energies are often so large that the associated degrees of freedom can usually be regarded as frozen out, particularly at low frequencies, where screening is dominated by the conduction electrons. However, in certain situations and for certain materials, core polarization can play an important role. For example, the metals Cd and In possess relatively shallow d states whose binding energies are of the same order of magnitude as the free-electron plasmon energy, $\hbar\omega_p^0$, where the characteristic plasmon frequency, $\omega_p^0=(4\pi n_v e^2/m)^{1/2}$, is determined by the mean valence electron density n_v. An interplay between the dynamic response of the core and valence electrons is then to be expected. Thus, while the electron-energy-loss spectra of these metals reveal well-defined plasmon excitations, the corresponding plasmon frequency is strongly shifted from the free-electron value. That these deviations arise in part from the polarization of the ionic cores is consistent with the observed trend on going from Cd to Sn. The decreasing frequency shift observed correlates with the decrease in core polarizability that would be expected as the $4d$ core band progressively narrows and moves away from the nearly-free-electron conduction bands. It is with this interplay of the core and conduction electron responses that we are concerned in this paper. The theory we present confirms the physical picture just described and detailed calculations of the dielectric response of these metals are found to yield plasma frequencies in good agreement with experiment. A preliminary account of our results was published previously.[1]

In earlier work, the free-ion polarizability was commonly used to estimate the effect of core polarization on the plasmon frequency of the alkali metals.[2] The basic idea is to view the ion cores in a metal as giving rise to an independent polarizable background which is characterized by a uniform frequency-independent dielectric constant, ϵ_0.[3] Taking the polarization of the background into account shifts the plasma frequency down to the value $\omega_p^0/\sqrt{\epsilon_0}$. This, however, constitutes an *ad hoc* extension of the usual theory of plasmons in metals in that core electrons are treated on a completely different footing from those comprising the conduction band. Although the approach is qualitatively correct, it is difficult to make it quantitative since there is no obvious prescription for choosing either the core polarizabilities or the

corresponding dielectric constant.

The polarizability of an ion in a metallic environment is in fact different from the free-ion polarizability for a number of reasons. Metallic screening leads to shifts in core levels, concomitant changes in excitation energies, and an altered set of available final states due to the formation of a conduction band with a sharp Fermi cutoff. These have important implications for both the core- and conduction-electron responses. For example, the core polarizability acquires a logarithmic singularity at a frequency corresponding to transitions from the core state to the Fermi level, which appears as structure in the optical absorption at these threshold energies. In addition, the core excitation oscillator strengths are modified by the exclusion of transitions to the occupied valence states. The f sum rule provides a useful measure of this effect and defines an effective core-electron charge density in the solid which is reduced from the expected free-ion contribution, n_c, because of the occupied conduction band. Conversely, the effective density of valence electrons is enhanced above the value implied by the atomic valence in order that the total sum rule be fulfilled. The enhanced valence electron density provides an upward shift of the plasma frequency which is overlooked when the core and conduction electrons are viewed as independent components. Accordingly, there are two opposing effects arising from the presence of core electrons which strike a delicate balance in determining the observed plasma frequency.

The question of enhancement of the valence response due to the core is closely linked to the question of core orthogonalization of the valence states, which is an important aspect exploited in pseudopotential theory.[4] Explicit use of core orthogonalization allows one to simplify electronic-structure calculations since core states are effectively eliminated and a relatively weak potential, the pseudopotential, is gained. In this way, pseudopotential theory provides a simple explanation for why a nearly-free-electron theory is a meaningful approximation for the valence electrons in simple metals and semiconductors. Although useful for many purposes, pseudopotential theory must be applied prudently in the context of optical absorption. The effect of the orthogonalization term on the oscillator strengths of interband transitions in simple metals has been considered[5–8] and in general an enhancement is predicted relative to calculations of matrix elements using pseudo-wave-functions. The importance of the core orthogonalization effect and thus the enhancement is expected intuitively to correlate with the size of the core relative to the atomic volume, but even for the alkali metals[8] the effect is significant.

Our purpose in this paper is to develop a theory of the electronic response of metals which simultaneously accounts for both the relatively localized core states forming a narrow filled band and the delocalized nearly-free-electron-like states of the conduction band. The disparate character of the two kinds of states necessitates different approximations in the evaluation of the respective core and valence response functions. The definition of these functions is taken up in Sec. II. The macroscopic dielectric function is then derived within the random-phase approximation in the long-wavelength limit. The detailed methods by which the response functions are calculated are outlined in Secs. III and IV for the core and valence electrons, respectively. In Sec. IV we pay attention in particular to the question discussed above of the enhancement of the valence electron oscillator strength. Thus while retaining the form of the valence response function suggested by pseudopotential theory, the valence interband oscillator strength is scaled by an amount consistent with the requirements of the f sum rule. Section V presents our results for various simple metals and comparison is made with experiment. Section VI contains our conclusions.

Although the main focus in our work is on obtaining an estimate of the plasma frequency, the method yields more generally the frequency-dependent dielectric function which can be used to interpret a variety of experimental observations, including optical data and electron-energy-loss measurements. In addition, our formalism can be applied to other problems involving the dynamical properties of core electrons such as those leading to the van der Waals interaction between the ion cores in metals.[9,10]

II. THE MACROSCOPIC DIELECTRIC FUNCTION

The combined treatment of the response properties of electrons comprising both highly localized core and delocalized conduction states is complicated by the very different nature of these states. One method for dealing with this problem was developed by Hedin,[11] who introduced a separation of the electronic system into core and valence components through the assignment of appropriate partial response functions. Once these response functions have been properly defined, the total response of the system to an external potential can then be calculated self-consistently by allowing the charge-density fluctuations of the core and valence electrons to interact through their mutual fields. As we shall see, the essential picture which emerges is one of localized induced dipoles immersed in and interacting with a gas of Bloch valence electrons.

The electronic response of a system to an external longitudinal perturbation can be characterized in terms of a microscopic dielectric function defined by the equation

$$\phi^{\text{ext}}(\mathbf{r},\omega)=\int d\mathbf{r}'\epsilon(\mathbf{r},\mathbf{r}',\omega)\phi^{\text{tot}}(\mathbf{r}',\omega)\ , \tag{2.1}$$

where ϕ^{ext} is the externally applied potential and ϕ^{tot} is the sum of the external and induced, ϕ^{ind}, electrostatic potentials. Since ϵ is invariant with respect to lattice translations in a periodic solid, (2.1) can be Fourier analyzed with the result

$$\phi^{\text{ext}}_{\mathbf{G}}(\mathbf{q},\omega)=\sum_{\mathbf{G}'}\epsilon_{\mathbf{G}\mathbf{G}'}(\mathbf{q},\omega)\phi^{\text{tot}}_{\mathbf{G}'}(\mathbf{q},\omega)\ , \tag{2.2}$$

where we have assumed a plane-wave spatial dependence of the external potential, $\phi^{\text{ext}}(\mathbf{r},t)=\phi^{\text{ext}}(\mathbf{q},\omega)e^{i(\mathbf{q}\cdot\mathbf{r}-\omega t)}$. The dielectric function appearing in (2.2) can be regarded as a matrix in reciprocal space. It is this property which gives rise to induced fields having wavelengths other than that of the external driving field.

In the following, we restrict our attention to metals with cubic symmetry. (Although some noncubic metals are considered, we approximate these by close-packed cubic solids). The long-wavelength macroscopic dielectric function is then defined quite generally by[12,13]

$$\epsilon_M(\omega)=\lim_{\mathbf{q}\to 0}\phi^{\rm ext}_{\mathbf{G}=0}(\mathbf{q},\omega)/\phi^{\rm tot}_{\mathbf{G}=0}(\mathbf{q},\omega)$$
$$=\lim_{\mathbf{q}\to 0}[\epsilon^{-1}_{\mathbf{G}=0,\mathbf{G}'=0}(\mathbf{q},\omega)]^{-1} . \quad (2.3)$$

As is well known, it is given in terms of the $\mathbf{G}=\mathbf{G}'=0$ component of the inverse microscopic dielectric function. The expression in terms of the potential Fourier components, however, is more convenient for our purposes.

To evaluate the dielectric function we adopt the random phase approximation (RPA) (Ref. 3), which is commonly used in these contexts. It should be pointed out, however, that the theory can easily be extended to include a local exchange and correlation potential as used in the time-dependent generalization[14] of density-functional theory (DFT).[15,16] Within the RPA the charge density induced by the external potential $\phi^{\rm ext}$ is determined by the set of equations

$$\delta\rho(\mathbf{r},\omega)=\int d^3r'\chi^0(\mathbf{r},\mathbf{r}',\omega)\phi^{\rm tot}(\mathbf{r}',\omega) , \quad (2.4)$$

with

$$\phi^{\rm tot}(\mathbf{r},\omega)=\phi^{\rm ext}(\mathbf{r},\omega)+\int d^3r'\delta\rho(\mathbf{r}',\omega)/|\mathbf{r}-\mathbf{r}'| . \quad (2.5)$$

If time-dependent DFT is to be employed, $\phi^{\rm tot}$ in (2.4) is replaced by the total Kohn-Sham potential which includes both the Coulomb interaction and an exchange-correlation contribution.

The function $\chi^0(\mathbf{r},\mathbf{r}',\omega)$ appearing in (2.4) is the independent-particle density response function of the solid and can be expressed in a number of equivalent ways. For example, it can be written in terms of the single-particle Green function as (invoking time-reversal symmetry)

$$\chi^0(\mathbf{r},\mathbf{r}',\omega)=2\sum_{\substack{n,\mathbf{k}\\(\rm occ)}}\psi^*_{n\mathbf{k}}(\mathbf{r})\psi_{n\mathbf{k}}(\mathbf{r}')$$
$$\times[G(\mathbf{r},\mathbf{r}',E_{n\mathbf{k}}+\hbar\omega)$$
$$+G^*(\mathbf{r},\mathbf{r}',E_{n\mathbf{k}}-\hbar\omega)] , \quad (2.6)$$

where

$$G(\mathbf{r},\mathbf{r}',E)=\sum_{n,\mathbf{k}}\frac{\psi_{n\mathbf{k}}(\mathbf{r})\psi^*_{n\mathbf{k}}(\mathbf{r}')}{E-E_{n\mathbf{k}}+i\delta} . \quad (2.7)$$

The summation in (2.6) extends only over the occupied Bloch states $\psi_{n\mathbf{k}}(\mathbf{r})$ with band energy $E_{n\mathbf{k}}$, while in (2.7) the summation also includes unoccupied states. The factor of 2 in (2.6) accounts for electron spin. The band states to be used in these calculations are in principle those obtained from a self-consistent band-structure calculation using, for example, the local density approximation of DFT.

Since the terms in the Green-function summation which correspond to occupied states do not in fact contribute to the response function, the latter can also be expressed as

$$\chi^0(\mathbf{r},\mathbf{r}',\omega)=2\sum_{\substack{n,\mathbf{k}\\(\rm occ)}}\psi^*_{n\mathbf{k}}(\mathbf{r})\psi_{n\mathbf{k}}(\mathbf{r}')f(\mathbf{r},\mathbf{r}',E_{n\mathbf{k}},\omega) , \quad (2.8)$$

where the factor $f(\mathbf{r},\mathbf{r}',E_{n\mathbf{k}},\omega)$ is given by

$$f(\mathbf{r},\mathbf{r}',E,\omega)=\sum_{\substack{m,\mathbf{k}'\\(\rm unocc)}}\left[\frac{\psi_{m\mathbf{k}'}(\mathbf{r})\psi^*_{m\mathbf{k}'}(\mathbf{r}')}{E+\hbar\omega-E_{m\mathbf{k}'}+i\delta}\right.$$
$$\left.+\frac{\psi^*_{m\mathbf{k}'}(\mathbf{r})\psi_{m\mathbf{k}'}(\mathbf{r}')}{E-\hbar\omega-E_{m\mathbf{k}'}-i\delta}\right] . \quad (2.9)$$

The particular form of the response function chosen is a matter of convenience.

We now split the sum over all occupied states in (2.8) into two groups, one containing the core bands and a second containing the occupied valence states. Doing so we obtain

$$\chi^0(\mathbf{r},\mathbf{r}',\omega)=\chi^0_c(\mathbf{r},\mathbf{r}',\omega)+\chi^0_v(\mathbf{r},\mathbf{r}',\omega) , \quad (2.10)$$

where the subscripts c and v denote the core- and valence-band contributions, respectively. The substitution of (2.10) into (2.4) implies that the induced charge density can be written as

$$\delta\rho(\mathbf{r},\omega)=\delta\rho_c(\mathbf{r},\omega)+\delta\rho_v(\mathbf{r},\omega) . \quad (2.11)$$

The utility of this decomposition will become apparent when the specific form of each of these density fluctuations is considered.

For the weakly overlapping core states of interest, the core-band wave functions can be expressed as tight-binding linear combinations of atomic orbitals $\phi_\alpha(\mathbf{r})$,

$$\psi_{n\mathbf{k}}(\mathbf{r})=N^{-1/2}\sum_{\alpha,\mathbf{R}}e^{i\mathbf{k}\cdot\mathbf{R}}b_{n\alpha}\phi_\alpha(\mathbf{r}-\mathbf{R}) . \quad (2.12)$$

We have assumed a Bravais lattice with lattice vectors $\mathbf{R}$; the index α denotes the full complement of atomic quantum numbers. We note that the function $f(\mathbf{r},\mathbf{r}',E_{n\mathbf{k}},\omega)$ depends on $\mathbf{k}$ only through the band energies $E_{n\mathbf{k}}$. Thus if the dispersion of the core bands is neglected, $E_{n\mathbf{k}}$ is equal to the atomic eigenvalue, E_α, and f is effectively independent of $\mathbf{k}$. Using this fact and the tight-binding form of the wave functions, the wave-vector summation in $\chi^0_c(\mathbf{r},\mathbf{r}',\omega)$ can be performed with the result

$$\chi^0_c(\mathbf{r},\mathbf{r}',\omega)=2\sum_{\substack{\mathbf{R}\\\alpha(\rm core)}}\phi^*_\alpha(\mathbf{r}-\mathbf{R})\phi_\alpha(\mathbf{r}'-\mathbf{R})f(\mathbf{r},\mathbf{r}',E_\alpha,\omega)$$
$$=\sum_{\mathbf{R}}\chi^0_a(\mathbf{r}-\mathbf{R},\mathbf{r}'-\mathbf{R},\omega) , \quad (2.13)$$

where $\chi^0_a(\mathbf{r}-\mathbf{R},\mathbf{r}'-\mathbf{R},\omega)$ is an atomiclike response function localized on the site $\mathbf{R}$. Details concerning the evaluation of this function are given in Sec. III, but for the present it is sufficient to realize that, because of the form of χ^0_c, the core charge-density fluctuation is given as a sum over lattice sites,

$$\delta\rho_c(\mathbf{r},\omega)=\sum_{\mathbf{R}}\delta\rho_{\mathbf{R}}(\mathbf{r},\omega) , \quad (2.14)$$

where $\delta\rho_{\mathbf{R}}$ is the induced core charge density at the site $\mathbf{R}$.

It is clear from (2.13) that $\delta\rho_{\mathbf{R}}$ has the same degree of localization as the core orbitals and is given explicitly by

$$\delta\rho_{\mathbf{R}}(\mathbf{r},\omega)=\int d^3r'\chi_a^0(\mathbf{r}-\mathbf{R},\mathbf{r}'-\mathbf{R},\omega)\phi^{\rm tot}(\mathbf{r}',\omega)\ . \tag{2.15}$$

Since

$$\phi^{\rm tot}(\mathbf{r}+\mathbf{R},\omega)=e^{i\mathbf{q}\cdot\mathbf{R}}\phi^{\rm tot}(\mathbf{r},\omega)\ , \tag{2.16}$$

we have

$$\delta\rho_{\mathbf{R}}(\mathbf{r}+\mathbf{R},\omega)=e^{i\mathbf{q}\cdot\mathbf{R}}\delta\rho_0(\mathbf{r},\omega)\ . \tag{2.17}$$

It is therefore sufficient to consider $\mathbf{R}=0$ in (2.15).

The total potential driving the core charge fluctuation on the site $\mathbf{R}$ is made up of four contributions: (i) the external potential, (ii) the induced potential due to all other core charges $\delta\rho_{\mathbf{R}'}(\mathbf{r},\omega)(\mathbf{R}'\neq\mathbf{R})$, (iii) the induced potential due to the valence charge density $\delta\rho_v(\mathbf{r},\omega)$, and (iv) the induced potential of $\delta\rho_{\mathbf{R}}$ itself. Contributions (i)–(iii) constitute an "external" local potential acting on the core at site $\mathbf{R}$. Because of the localized nature of the core, it is reasonable to assume that this external potential is slowly varying over the extent of the core and that it can therefore be expanded about the position of the central site ($\mathbf{R}=0$). To lowest order the core charge density on this site is determined by

$$\delta\rho_0(\mathbf{r},\omega)=\int d^3r'\chi_a^0(\mathbf{r},\mathbf{r}',\omega)[-\mathbf{r}'\cdot\mathbf{E}_0+\phi_0(\mathbf{r}',\omega)]\ , \tag{2.18}$$

where $\mathbf{E}_0=\mathbf{E}^{\rm loc}(\mathbf{r}=\mathbf{R}=0)$ is the local electric field at the site $\mathbf{R}=0$ due to all charges exclusive of $\delta\rho_0$ itself. ϕ_0, on the other hand, is the electric potential due to $\delta\rho_0$; (2.18) is therefore an integral equation for the induced core density, which has the same form as for an isolated atomic system. It should be noted, however, that the local field $\mathbf{E}_0$ depends implicitly on the magnitude of the core polarization and is not simply the externally imposed field.

In the approximation we use to evaluate the core response function (see Sec. III), χ_a^0 represents a system with spherical symmetry. It is thus convenient to define a vector polarization by the equation

$$\delta\rho_0(\mathbf{r},\omega)=\mathbf{p}_0(\mathbf{r},\omega)\cdot\mathbf{E}_0\ , \tag{2.19}$$

where $\mathbf{p}_0$ is a vector in the direction of $\mathbf{r}$. The induced dipole moment on the central site is then $\mathbf{d}_0=\alpha(\omega)\mathbf{E}_0$ which defines the core polarizability

$$\alpha(\omega)=\tfrac{1}{3}\int d^3r\ \mathbf{r}\cdot\mathbf{p}_0(\mathbf{r},\omega)\ . \tag{2.20}$$

It is this quantity which characterizes the dipolar response of the ion cores in the metal.

We now obtain the equations defining the Fourier amplitudes of the total potential, $\phi_{\mathbf{G}}^{\rm tot}(\mathbf{q},\omega)$. The Fourier transform of the valence charge density is given by

$$\delta\rho_v(\mathbf{q}+\mathbf{G},\omega)=\sum_{\mathbf{G}'}\chi_v^0(\mathbf{q}+\mathbf{G},\mathbf{q}+\mathbf{G}',\omega)\phi_{\mathbf{G}'}^{\rm tot}(\mathbf{q},\omega)\ , \tag{2.21}$$

where the response matrix is defined by

$$\chi_v^0(\mathbf{q}+\mathbf{G},\mathbf{q}+\mathbf{G}',\omega)=\frac{1}{V}\int d^3r\int d^3r' e^{-i(\mathbf{q}+\mathbf{G})\cdot\mathbf{r}}\times\chi_v^0(\mathbf{r},\mathbf{r}',\omega)e^{i(\mathbf{q}+\mathbf{G}')\cdot\mathbf{r}'}\ . \tag{2.22}$$

Similarly, using (2.14) and (2.19), the Fourier transform of the core charge density is

$$\delta\rho_c(\mathbf{q}+\mathbf{G},\omega)=n_i\mathbf{p}_0(\mathbf{q}+\mathbf{G},\omega)\cdot\mathbf{E}_0\ , \tag{2.23}$$

where n_i is the atomic density and

$$\mathbf{p}_0(\mathbf{q}+\mathbf{G},\omega)=\int d^3r\ \mathbf{p}_0(\mathbf{r},\omega)e^{-i(\mathbf{q}+\mathbf{G})\cdot\mathbf{r}}\ . \tag{2.24}$$

In terms of these quantities, $\phi_{\mathbf{G}}^{\rm tot}(\mathbf{q},\omega)$ satisfies the equation [with $\phi_{\mathbf{G}}^{\rm ext}(\mathbf{q},\omega)=\delta_{\mathbf{G},0}$]

$$\phi_{\mathbf{G}}^{\rm tot}(\mathbf{q},\omega)=\delta_{\mathbf{G},0}+\frac{4\pi}{|\mathbf{q}+\mathbf{G}|^2}\sum_{\mathbf{G}'}\chi_v^0(\mathbf{q}+\mathbf{G},\mathbf{q}+\mathbf{G}',\omega)\phi_{\mathbf{G}'}^{\rm tot}(\mathbf{q},\omega)+\frac{4\pi n_i}{|\mathbf{q}+\mathbf{G}|^2}\mathbf{p}_0(\mathbf{q}+\mathbf{G},\omega)\cdot\mathbf{E}_0\ . \tag{2.25}$$

To close this system of equations, the local external field must be related to the total field. It is given by

$$\mathbf{E}_0=-\nabla[\phi^{\rm tot}(\mathbf{r},\omega)-\phi_0(\mathbf{r},\omega)]_{\mathbf{r}=0}=-i\mathbf{q}-\sum_{\mathbf{G}}(\mathbf{q}+\mathbf{G})\frac{4\pi i}{|\mathbf{q}+\mathbf{G}|^2}\sum_{\mathbf{G}'}\chi_v^0(\mathbf{q}+\mathbf{G},\mathbf{q}+\mathbf{G}',\omega)\phi_{\mathbf{G}'}^{\rm tot}(\mathbf{q},\omega)+\alpha(\omega)\sum_{\mathbf{R}\neq0}\left[\frac{\mathbf{E}_0}{R^3}-\frac{3(\mathbf{E}_0\cdot\mathbf{R})\mathbf{R}}{R^5}\right]e^{i\mathbf{q}\cdot\mathbf{R}}\ . \tag{2.26}$$

The last term accounts for the dipolar fields from all other sites; in the limit $\mathbf{q}\to0$ for systems with cubic symmetry it reduces to $-(8\pi/3)n_i\alpha(\omega)\mathbf{E}_0$. We shall use this result since the final expressions are required only in this limit. Solving (2.26) for $\mathbf{E}_0$ and inserting the result into (2.25) yields (suppressing the explicit frequency dependence in the following)

$$\phi_{\mathbf{G}}^{\rm tot}(\mathbf{q})=\delta_{\mathbf{G},0}-\frac{4\pi n_i}{|\mathbf{q}+\mathbf{G}|^2}\frac{i\mathbf{q}\cdot\mathbf{p}_0(\mathbf{q}+\mathbf{G})}{1+8\pi n_i\alpha/3}-\sum_{\mathbf{G}'}[\underline{\epsilon}^v(\mathbf{q})-\underline{\mathbb{1}}]_{\mathbf{G}\mathbf{G}'}\phi_{\mathbf{G}'}^{\rm tot}(\mathbf{q})+\frac{4\pi n_i}{|\mathbf{q}+\mathbf{G}|^2}\frac{i\mathbf{p}_0(\mathbf{q}+\mathbf{G})}{1+8\pi n_i\alpha/3}\cdot\sum_{\mathbf{G}'\mathbf{G}''}(\mathbf{q}+\mathbf{G}')[\underline{\epsilon}^v(\mathbf{q})-\underline{\mathbb{1}}]_{\mathbf{G}'\mathbf{G}''}\phi_{\mathbf{G}''}^{\rm tot}(\mathbf{q})\ , \tag{2.27}$$

where we have introduced the valence dielectric function by

$$\epsilon_{\mathbf{G}\mathbf{G}'}^v(\mathbf{q})=\delta_{\mathbf{G}\mathbf{G}'}-\frac{4\pi}{|\mathbf{q}+\mathbf{G}|^2}\chi_v^0(\mathbf{q}+\mathbf{G},\mathbf{q}+\mathbf{G}')\ . \tag{2.28}$$

Defining its inverse by

$$[\underline{\epsilon}^{v}(\mathbf{q})]^{-1}\underline{\epsilon}^{v}(\mathbf{q})=\underline{1}\ , \tag{2.29}$$

Eq. (2.27) can be written in the form

$$\phi_{\mathbf{G}}^{\mathrm{tot}}(\mathbf{q})=[\underline{\epsilon}^{v}(\mathbf{q})]_{\mathbf{G}0}^{-1}-i\frac{4\pi n_i}{1+8\pi n_i\alpha/3}\sum_{\mathbf{G}'}[\underline{\epsilon}^{v}(\mathbf{q})]_{\mathbf{G}\mathbf{G}'}^{-1}\frac{\mathbf{q}\cdot\mathbf{p}_0(\mathbf{q}+\mathbf{G}')}{|\mathbf{q}+\mathbf{G}'|^2}[1-\Phi(\mathbf{q})]\ , \tag{2.30}$$

where the function $\Phi(\mathbf{q})$ is defined by

$$i\mathbf{q}\Phi(\mathbf{q})=\sum_{\mathbf{G}} i(\mathbf{q}+\mathbf{G})\left[\sum_{\mathbf{G}'}\epsilon_{\mathbf{G}\mathbf{G}'}^{v}(\mathbf{q})\phi_{\mathbf{G}'}^{\mathrm{tot}}(\mathbf{q})-\phi_{\mathbf{G}}^{\mathrm{tot}}(\mathbf{q})\right]\ . \tag{2.31}$$

We have noted explicitly that the vector quantity on the right-hand side vanishes in the $\mathbf{q}\rightarrow 0$ limit as is evident from the fact that the last term in (2.27) must have a finite limit when $\mathbf{G}=0$. Furthermore, for a cubic crystal, the vector must be in the same direction as $\mathbf{q}$. It is now a straightforward matter to substitute the expression for $\phi_{\mathbf{G}}^{\mathrm{tot}}(\mathbf{q})$ from (2.30) into (2.31) and to solve for $[1-\Phi(\mathbf{q})]$,

$$[1-\Phi(\mathbf{q})]=\sum_{\mathbf{G}'}\frac{\mathbf{q}\cdot(\mathbf{q}+\mathbf{G}')}{q^2}[\underline{\epsilon}^{v}(\mathbf{q})]_{\mathbf{G}'0}^{-1}\frac{1}{[1-\Lambda(\mathbf{q})]} \tag{2.32}$$

with

$$\Lambda(\mathbf{q})=\frac{4\pi n_i}{1+8\pi n_i\alpha/3}\sum_{\mathbf{G}}\frac{i\mathbf{q}\cdot(\mathbf{q}+\mathbf{G})}{q^2}\left[\frac{\mathbf{q}\cdot\mathbf{p}_0(\mathbf{q}+\mathbf{G})}{|\mathbf{q}+\mathbf{G}|^2}-\sum_{\mathbf{G}'}[\underline{\epsilon}^{v}(\mathbf{q})]_{\mathbf{G}\mathbf{G}'}^{-1}\frac{\mathbf{q}\cdot\mathbf{p}_0(\mathbf{q}+\mathbf{G}')}{|\mathbf{q}+\mathbf{G}'|^2}\right]\ . \tag{2.33}$$

The macroscopic dielectric function is thus given by

$$\epsilon_M(\omega)=\lim_{\mathbf{q}\rightarrow 0}\left[[\underline{\epsilon}^{v}(\mathbf{q})]_{00}^{-1}-i\frac{4\pi n_i}{1+8\pi n_i\alpha/3}\sum_{\mathbf{G}}[\underline{\epsilon}^{v}(\mathbf{q})]_{0\mathbf{G}}^{-1}\frac{\mathbf{q}\cdot\mathbf{p}_0(\mathbf{q}+\mathbf{G})}{|\mathbf{q}+\mathbf{G}|^2}[1-\Phi(\mathbf{q})]\right]^{-1}\ . \tag{2.34}$$

This is the exact formal solution of the problem defined by (2.4) and (2.5). The result is simplified if we make one final approximation motivated by the fact that the valence states in the metals of interest are free-electron-like. We expect local field effects with respect to the valence electron response to be relatively weak, in which case the off-diagonal matrix elements of the valence dielectric function can be neglected. We therefore take

$$[\underline{\epsilon}^{v}(\mathbf{q})]_{\mathbf{G}\mathbf{G}'}^{-1}\approx\frac{\delta_{\mathbf{G}\mathbf{G}'}}{[\underline{\epsilon}^{v}(\mathbf{q})]_{\mathbf{G}\mathbf{G}}}\ . \tag{2.35}$$

With this approximation, (2.34) reduces to (reintroducing the frequency dependence)

$$\epsilon_M(\omega)=\epsilon_{00}^{v}(\mathbf{q}\rightarrow 0,\omega)+\frac{4\pi n_i\alpha(\omega)}{1-\frac{4\pi n_i\alpha(\omega)}{3}\left[1+\sum_{\mathbf{G}\neq 0}f(G,\omega)[1-1/\epsilon_{\mathbf{G}\mathbf{G}}^{v}(\mathbf{0},\omega)]\right]}\ . \tag{2.36}$$

In arriving at this result we have used the fact that $\mathbf{p}_0(\mathbf{r},\omega)=\hat{\mathbf{r}}p_0(r,\omega)$ so that

$$\mathbf{p}_0(\mathbf{G},\omega)=-i\hat{G}p_0(G,\omega) \tag{2.37}$$

with

$$p_0(G,\omega)=4\pi\int_0^{\infty}dr\,r^2 j_1(Gr)p_0(r,\omega)\ . \tag{2.38}$$

Here, $j_n(x)$ is a spherical Bessel function of the first kind. In the small-G limit, (2.38) reduces to

$$p_0(G,\omega)\simeq G\alpha(\omega)\ . \tag{2.39}$$

The dipole form factor $f(G,\omega)$ appearing in (2.36) is defined in terms of these quantities as

$$f(G,\omega)=\frac{p_0(G,\omega)}{G\alpha(\omega)}\ , \tag{2.40}$$

which in general is a complex function decreasing with G from the value 1 at $\mathbf{G}=0$. In the point-dipole model treated earlier,[17] $f(G,\omega)=1$ for all G since the dipole has no spatial extent, and (2.36) is the same as the result obtained there. The main advantage of the present formulation, however, is the precise definition of the core polarizability $\alpha(\omega)$ which follows from the solution of the integral equation (2.18).

Although the valence-electron response has been approximated in this derivation, local-field effects with regard to the core-electron response are included completely as is evident from the Clausius-Mossotti (CM) form of the second term in (2.36). The modification to the usual CM expression is contained within the large parentheses in the denominator of (2.36); it accounts for the valence charge fluctuations induced by the short-wavelength "local fields" of the core dipoles.

III. THE CORE POLARIZABILITY $\alpha(\omega)$

The essential ingredient for calculating the core polarization $\mathbf{p}_0(\mathbf{r},\omega)$ used in the evaluation of $\alpha(\omega)$ is the independent-particle response function $\chi_a^0(\mathbf{r},\mathbf{r}',\omega)$ defined in (2.13) and (2.9). An efficient method for obtaining such response functions was developed recently and applied in a calculation of both the static[18] and dynamic[14] polarizability of closed-shell atoms and ions. In this method, the explicit evaluation of unoccupied states as required in (2.9) is circumvented by calculating directly the Green function appearing in (2.6). The calculation is straightforward for a spherically symmetric system but is considerably more difficult for a periodic solid. However, we shall argue that it is possible to reduce the calculation to the spherical situation for the core response properties of interest.

As mentioned in the Introduction, the essential difference between the polarizability of a free ion and an ion in a metal is the forbidden excitation of core electrons to final states which are occupied by valence electrons. This restriction can be represented in the short-hand notation [see (2.8)–(2.10)]

$$\chi_c^0(\mathbf{r},\mathbf{r}')=\sum_c \sum_{j\ (\text{unocc})} = \sum_c \sum_j - \sum_c \sum_v , \tag{3.1}$$

where c and v denote states in the core and valence bands, respectively. In the second line, the error incurred by summing j over all states is corrected by the explicit subtraction of core- to valence-band excitations. Contributions from final core states ($j=c$) cancel identically in (3.1). With (3.1), the atomic response function defined in (2.13) takes the form

$$\chi_a^0(\mathbf{r},\mathbf{r}',\omega)=\tilde{\chi}_a^0(\mathbf{r},\mathbf{r}',\omega)-\Delta\chi_a^0(\mathbf{r},\mathbf{r}',\omega) , \tag{3.2}$$

where

$$\tilde{\chi}_a^0(\mathbf{r},\mathbf{r}',\omega)=2\sum_\alpha \phi_\alpha^*(\mathbf{r})\phi_\alpha(\mathbf{r}')[G(\mathbf{r},\mathbf{r}',E_\alpha+\hbar\omega)+G^*(\mathbf{r},\mathbf{r}',E_\alpha-\hbar\omega)] , \tag{3.3}$$

$$\Delta\chi_a^0(\mathbf{r},\mathbf{r}',\omega)=2\sum_\alpha \phi_\alpha^*(\mathbf{r})\phi_\alpha(\mathbf{r}')\Delta f(\mathbf{r},\mathbf{r}',E_\alpha,\omega) , \tag{3.4}$$

and

$$\Delta f(\mathbf{r},\mathbf{r}'E_\alpha,\omega)=\sum_v \left[\frac{\psi_v(\mathbf{r})\psi_v^*(\mathbf{r}')}{E_\alpha+\hbar\omega-E_v+i\delta} + \frac{\psi_v^*(\mathbf{r})\psi_v(\mathbf{r}')}{E_\alpha-\hbar\omega-E_v-i\delta} \right] . \tag{3.5}$$

Although the expression for $\tilde{\chi}_a^0$ has the appearance of a free-ion response function, it should be noted that the Green function appearing is the full lattice Green function. $\tilde{\chi}_a^0$ describes the response of a fictitious solid in which only the core bands are occupied. The correction $\Delta\chi_a^0$ accounts for the valence-band occupancy.

The lattice Green function provides the total probability amplitude for propagating from $\mathbf{r}'$ to $\mathbf{r}$ and in general includes multiple scattering from each of the ions in the lattice. However, since the core states $\phi_\alpha(\mathbf{r})$ are assumed to be localized, the Green function in (3.3) is only required for values of its arguments within the region of a single site. In this situation, the Green function can be developed in a series of the form

$$G=G_0+G_0t_0G_0+\cdots , \tag{3.6}$$

where G_0 is the free-space propagator and t_0 is the central site t matrix. The remaining terms in the series represent scattering from all other sites. For the frequencies of interest, $E_\alpha+\hbar\omega$ corresponds to an energy in the conduction band; at these energies, electrons propagate essentially as free particles as evidenced by the nearly-free-electron energy dispersion.[19] This implies that the scattering induced by the ionic potential is relatively weak and it is therefore a good approximation to neglect all terms in the series other than the central site contribution. Within this site it is of course necessary to include the full ionic potential since the propagator deviates strongly from its free-space form. For the energy $E_\alpha-\hbar\omega$, the propagator attenuates exponentially with separation and the central site contribution again dominates.

These observations motivate our single-site approximation whereby the ion in the central cell is viewed as an impurity in an otherwise homogeneous electron gas having a density equal to the mean conduction electron density of the metal. Such an approximation was first introduced by Dagens[20] and has been used subsequently in other contexts.[21] It is especially appropriate when the properties of interest are dominated by the local electronic environment.[22] We therefore adopt a model in which the central ion is placed into a vacancy created by removing the positive background charge within a spherical volume containing the valence charge of the ion. The electronic structure for this situation is calculated self-consistently using density-functional theory[15,16] in the local-density approximation.[23] This amounts to solving the single-particle Schrödinger equation

$$\left[-\frac{\hbar^2}{2m}\nabla^2+v_{\text{eff}}(\mathbf{r})-E_i \right]\psi_i(\mathbf{r})=0 , \tag{3.7}$$

where

$$v_{\text{eff}}(\mathbf{r})=-\frac{Z}{r}+v_{\text{vac}}(\mathbf{r})+\int d^3r'\frac{n(\mathbf{r}')}{|\mathbf{r}-\mathbf{r}'|}+v_{\text{xc}}(\mathbf{r}) . \tag{3.8}$$

Z is the nuclear charge, v_{vac} is the electrostatic potential of the vacancy, and $v_{\text{xc}}(\mathbf{r})$ is the exchange-correlation potential. The total electronic density is then given by

$$n(\mathbf{r})=2\sum_i |\psi_i|^2 . \tag{3.9}$$

Both core and conduction states are defined in terms of a common self-consistent potential, v_{eff}. The core electrons therefore find themselves in an environment characteristic of the metallic state in that the ionic potential is

screened by conduction electrons rather than discrete valence states. The extent to which the approximations we have made are reasonable can be judged by comparing the position of core levels as determined here with self-consistent band-structure calculations.[19] For example, the 4*d* core level of In in our model is 15.8 eV below the Fermi energy while the 4*d* core band in the band-structure calculations has a width of about 0.6 eV and is centered 15.6 eV below the Fermi energy. It is therefore clear that the single-site approximation simulates very nicely the electronic structure of the ion core. This also applies to the conduction states. The observation that the scattering phase shifts are all close to multiples of π confirms the relatively weak scattering power of the self-consistent potentials and accounts for the free-electron-like behavior.

Because of the spherical symmetry of the self-consistent potential, the core and valence states have the form

$$\psi_c(\mathbf{r})=R_{nl}(r)Y_{lm}(\hat{\mathbf{r}}) , \tag{3.10}$$

$$\psi_v(\mathbf{r})=R_{kl}(r)Y_{lm}(\hat{\mathbf{r}}) , \tag{3.11}$$

where Y_{lm} is a spherical harmonic and $R(r)$ is a radial wave function. The core states are required to construct the response function $\tilde{\chi}_a$ and the single-site Green function can be calculated as in the atomic problem[18] once the ionic potential has been specified. $\tilde{\chi}_a$ thus has the same structure as for a free ion, but the potential defining the ion core does not support additional bound valence states since these have been pushed up into the continuum. The nature of the external field in (2.18) requires the calculation of only the dipolar component of the spherical harmonic expansion of $\tilde{\chi}_a$ [see (3.12) below]; an explicit expression for this quantity can be found in Ref. 18.

The correction $\Delta\chi_a^0$ is a new feature in the present problem and requires the evaluation of Δf. It too has a spherical harmonic expansion of the form

$$\Delta\chi_a^0(\mathbf{r},\mathbf{r}',\omega)=\sum_L \Delta\chi_a^{(l)}(r,r',\omega)Y_{lm}^*(\hat{\mathbf{r}})Y_{lm}(\hat{\mathbf{r}}') . \tag{3.12}$$

Using the wave functions in Eqs. (3.10) and (3.11), we have

$$\Delta\chi_a^{(l)}(r,r',\omega)=2\sum_{nl'}\sum_{kl''}C_{ll'l''}R_{nl'}(r)R_{nl'}(r')R_{kl''}(r)R_{kl''}(r')\left[\frac{1}{E_{nl'}-E_k+\omega+i\delta}+\frac{1}{E_{nl'}-E_k-\omega-i\delta}\right] , \tag{3.13}$$

where

$$C_{ll'l''}=\left[\frac{(2l'+1)(2l''+1)}{4\pi(2l+1)}\right]^{1/2}\times\int d\hat{\mathbf{x}}Y_{l0}(\hat{\mathbf{x}})Y_{l'0}(\hat{\mathbf{x}})Y_{l''0}(\hat{\mathbf{x}}) . \tag{3.14}$$

Here, $E_k=k^2/2$. Since only the dipolar response is required, we can set $l=1$ in (3.13).

We now define

$$\Delta f_l^{(1)}(r,r',\omega)=\sum_{kl'}C_{1ll'}R_{kl'}(r)R_{kl'}(r')\frac{1}{\omega-E_k+i\delta} \tag{3.15}$$

whose imaginary part is given by

$$\mathrm{Im}\Delta f_l^{(1)}(r,r',\omega)=-\pi\sum_{kl'}C_{1ll'}R_{kl'}(r)R_{kl'}(r')\delta(\omega-E_k) . \tag{3.16}$$

The real part can be obtained by a Kramers-Kronig relation. In terms of $\Delta f_l^{(1)}$, $\Delta\chi_a^{(1)}$ is given by

$$\Delta\chi_a^{(1)}(r,r',\omega)=2\sum_{nl}R_{nl}(r)R_{nl}(r')\times[\Delta f_l^{(1)}(r,r',E_{nl}+\omega)+\Delta f_l^{(1)}(r,r',E_{nl}-\omega)^*] . \tag{3.17}$$

We assume that the scattering state $R_{kl}(r)$ is normalized within a large sphere of radius R. The wave vectors are then specified by $k=k_n=n\pi/R$ with n a positive integer. The k summation is performed by replacing $\sum_k\cdots$ by $(R/\pi)\int_0^\infty dk\ldots$, and we obtain

$$\mathrm{Im}\Delta f_l^{(1)}(r,r',\omega)=-2k_0\sum_{l'}C_{1ll'}R_{k_0l'}(r)R_{k_0l'}(r')\times\Theta(E_F-\omega) \tag{3.18}$$

with $k_0=\sqrt{2\omega}$. The normalization of the radial wave function is now defined by the asymptotic condition

$$R_{kl}(r)\to\frac{\sin[kr-\frac{1}{2}\pi l-\delta_l(k)]}{kr} \tag{3.19}$$

at large r. The sum over l' contains two terms, $l'=l\pm1$, due to the dipole selection rule. The real part of $\Delta f_l^{(1)}(r,r',\omega)$ is finally obtained from

$$\mathrm{Re}\Delta f_l^{(1)}(r,r',\omega)=P\int\frac{d\omega'}{\pi}\frac{\mathrm{Im}\Delta f_l^{(1)}(r,r',\omega')}{\omega'-\omega} . \tag{3.20}$$

The spectral density given in Eq. (3.18) is finite only in the range $0\le\omega'\le E_F$. To be consistent with the evaluation of the Green function, the radial wave functions at energy ω' are obtained by numerical solution of the radial Schrödinger equation in the single-site approximation. Since the principal value integral is evaluated numerically, the singularity is treated by adding and subtracting the value of the spectral density at $\omega=\omega'$, $\mathrm{Im}\Delta f_l^{(1)}(r,r',\omega)$, and performing the remaining principal part integral analytically.

The induced charge density in the central cell is obtained by numerical solution of the integral equation (2.18) with the atomic response function defined in this section. In order to include exchange-correlation effects within the core, the electrostatic potential in (2.18) was augmented by the change in exchange-correlation poten-

tial as in earlier atomic calculations.[18] This generalization is not entirely consistent with the RPA level of approximation which was used to treat core-valence interactions, but by doing so the ionic response properties are represented more accurately. However, the inclusion of exchange and correlation in the atomic response calculation is known to be of only secondary importance,[14,18] and its neglect would not alter our present results appreciably.

The behavior of the core polarizability $\alpha(\omega)$ is illustrated for the example of In in Fig. 1. Also shown for comparison is the independent-particle polarizability $\alpha_0(\omega)$ which is obtained by excluding the electronic interaction terms in (2.18). It can be seen that the effect of the internal screening fields is significant, reducing the static polarizability by approximately 30%. The core polarizability also differs from the free-ion polarizability which has the static value 3.36 a.u. as compared with $\alpha(0)=3.9$ a.u. obtained here. Nieminen and Puska[24] have also considered core polarizabilities in metals, but their results have been obtained neglecting the correction $\Delta\chi_a^0$ in (3.2). As a result, they find a value of 5.33 a.u. for the polarizability of the In core in the metal. The difference between 5.33 and 3.9 a.u. is due to the restriction on core excitations to energies above the Fermi level and is seen to reduce considerably the magnitude of the core polarizability. Finally, the difference between 3.36 a.u. as obtained for the free ion and 5.33 a.u. for the ion in the metal shows the effect of metallic screening; in the metal the core states are shallower relative to the conduction-band minimum and are therefore more polarizable.

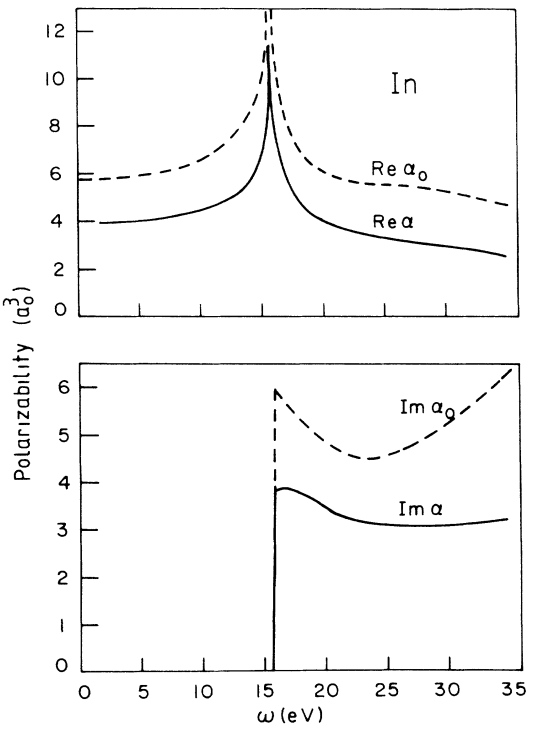

FIG. 1. Core polarizability of indium (in atomic units, a_0^3) vs frequency (in electronvolts). α_0 is the independent particle polarizability and α is the total core polarizability including interactions.

Since all the states below the Fermi level are occupied, the imaginary part of $\alpha(\omega)$ is zero below the threshold frequency $\omega_T=E_F-E_{4d}$ at which the $4d$ core level can first be excited. Accordingly, the real part of $\alpha(\omega)$ acquires a logarithmic singularity at this frequency. This is the most notable modification of the core polarizability and, as will be discussed in Sec. V, this feature is reflected in the behavior of the dielectric function in the vicinity of the core excitation threshold.

IV. THE VALENCE RESPONSE FUNCTION

The approximate macroscopic dielectric function derived in Sec. II depends only on the diagonal matrix elements of the valence dielectric function defined in (2.28). Retaining only the diagonal elements is equivalent to neglecting local-field effects within the valence electron system which therefore is assumed to be effectively homogeneous. The elements $\epsilon_{00}^v(\mathbf{q},\omega)$ and $\epsilon_{\mathbf{GG}}^v(\mathbf{q},\omega)$ for $\mathbf{G}\neq 0$ enter in different ways, as is obvious by inspection of (2.36). Whereas $\epsilon_{00}^v(\mathbf{q},\omega)$ gives the direct response of the valence electrons to the total field at wave vector $\mathbf{q}$, the elements $\epsilon_{\mathbf{GG}}^v(\mathbf{q},\omega)$ account for the way in which these electrons respond to the shorter-wavelength Fourier components arising from the localized core dipole moments. Since $\epsilon_{\mathbf{GG}}^v(\mathbf{q},\omega)$ contributes to the denominator of the effective core response function in an averaged way, the fine structure associated with details of the band structure is not expected to be important. One should therefore be able to approximate $\epsilon_{\mathbf{GG}}^v(\mathbf{q},\omega)$ by the free-particle dielectric function but modified in such a way as to be consistent with the presence of core electrons.

To understand this in more detail and to obtain a quantitative measure of the effect of core electrons, we consider the f sum rule for the valence electrons expressed in the form

$$\int_0^\infty \frac{d\omega}{\pi}\omega\,\mathrm{Im}\chi_v^0(\mathbf{q}+\mathbf{G},\mathbf{q}+\mathbf{G},\omega) = -\tfrac{1}{2}(\mathbf{q}+\mathbf{G})^2 n_v^{\mathrm{eff}}(\mathbf{q}+\mathbf{G})\ . \quad (4.1)$$

This equation defines an effective valence electron density $n_v^{\mathrm{eff}}(\mathbf{q}+\mathbf{G})$ which differs from the nominal valence density because of the existence of core electrons. [$n_v^{\mathrm{eff}}(\mathbf{q}+\mathbf{G})$ should not be confused with the Fourier transform of the valence electron density.] It is evaluated using the expressions of Sec. II which give

$$\chi_v^0(\mathbf{q}+\mathbf{G},\mathbf{q}+\mathbf{G},\omega)=\frac{2}{V}\sum_v\sum_{j>v}|M_{vj}(\mathbf{q}+\mathbf{G})|^2 \times\frac{2(E_v-E_j)}{(E_v-E_j)^2+(\omega+i\delta)^2}\ , \quad (4.2)$$

where $M_{ij}(\mathbf{q}+\mathbf{G})=\langle i|\exp[-i(\mathbf{q}+\mathbf{G})\cdot r]|j\rangle$. By adding and subtracting core and valence states, the double sum can be regrouped as indicated below:

$$\sum_v \left[\sum_{j>v}\right]=\sum_{c,v}\left[\sum_{j>v}\right]-\sum_c\left[\sum_{j>v}\right]$$
$$=\sum_{c,v}\left[\sum_j\right]-\sum_c\left[\sum_{j>c}-\sum_v\right]$$
$$=\sum_{c,v}\left[\sum_j\right]-\sum_c\left[\sum_j\right]+\sum_c\left[\sum_v\right]. \quad (4.3)$$

The first term represents the total response function, the second a response function for which only the core bands are occupied, and the last accounts for transitions from the core bands to the occupied valence states. Substituting the imaginary part of these expressions into (4.1), we obtain

$$\tfrac{1}{2}(\mathbf{q}+\mathbf{G})^2 n_v^{\rm eff}(\mathbf{q}+\mathbf{G})=\tfrac{1}{2}(\mathbf{q}+\mathbf{G})^2(n_v+n_c)-\tfrac{1}{2}(\mathbf{q}+\mathbf{G})^2 n_c-\frac{2}{V}\sum_c\sum_v |M_{cv}(\mathbf{q}+\mathbf{G})|^2(E_c-E_v)$$
$$=\tfrac{1}{2}(\mathbf{q}+\mathbf{G})^2 n_v-\int_0^\infty \frac{d\omega}{\pi}\omega\,\mathrm{Im}\Delta\chi_c^0(\mathbf{q}+\mathbf{G},\mathbf{q}+\mathbf{G},\omega)\,, \quad (4.4)$$

where

$$\Delta\chi_c^0(\mathbf{q}+\mathbf{G},\mathbf{q}+\mathbf{G},\omega)=\frac{1}{V}\int d^3r\int d^3r' e^{-i(\mathbf{q}+\mathbf{G})\cdot(\mathbf{r}-\mathbf{r}')}\sum_{\mathbf{R}}\Delta\chi_a^0(\mathbf{r}-\mathbf{R},\mathbf{r}'-\mathbf{R},\omega)$$
$$=n_i\int d^3r\int d^3r' e^{-i(\mathbf{q}+\mathbf{G})\cdot(\mathbf{r}-\mathbf{r}')}\Delta\chi_a^0(\mathbf{r},\mathbf{r}',\omega)\,. \quad (4.5)$$

$\Delta\chi_a^0(\mathbf{r},\mathbf{r}',\omega)$ was evaluated in the last section, but we note that all terms in the expansion in (3.12) contribute here, not just the $l=1$ term, as in (3.17). Since $E_c<E_v$, the core-valence oscillator strength in (4.4) gives a positive contribution that enhances the effective valence electron density.

Using (4.5) and expanding the plane-wave factors in spherical harmonics, we find

$$\int_0^\infty \frac{d\omega}{\pi}\omega\,\mathrm{Im}\Delta\chi_c^0(\mathbf{q}+\mathbf{G},\mathbf{q}+\mathbf{G},\omega)=\frac{4n_i}{\pi}\int_0^{k_F} dk\,k^2\sum_l\sum_{nl'}\sum_{l''}\tilde{C}_{ll'l''}(E_{nl'}-E_k)\left[\int_0^\infty dr\,r^2 j_l(Kr)R_{nl'}(r)R_{kl''}(r)\right]^2 \quad (4.6)$$

with $K=|\mathbf{q}+\mathbf{G}|$ and $\tilde{C}_{ll'l''}=4\pi(2l+1)C_{ll'l''}$. For $\mathbf{G}=0$ and for small $\mathbf{q}$, (4.6) reduces to

$$\int_0^\infty \frac{d\omega}{\pi}\omega\,\mathrm{Im}\Delta\chi_c^0(\mathbf{q},\mathbf{q},\omega)=q^2\frac{4n_i}{9\pi}\int_0^{k_F} dk\,k^2\sum_{nl'}\sum_{l''}\tilde{C}_{1l'l''}(E_{nl'}-E_k)\left[\int_0^\infty dr\,r^3 R_{nl'}(r)R_{kl''}(r)\right]^2, \quad (4.7)$$

which involves only dipole matrix elements between the core and valence states.

The f sum rule excess $n_v^{\rm eff}(G)-n_v$ is plotted in Fig. 2 for the case of In and is given in Table I for all the metals considered. It is seen to be a significant correction, particularly for atoms with large cores. In spite of the single-site approximation, we expect our results for this quantity to be accurate for two reasons. First, the valence-band structure is not perturbed severely from the free-particle form, and second, the valence-band scattering states produce a total screening charge for each ion which has the correct magnitude since the Friedel sum rule is satisfied. The amplitude of the valence states within the central cell is therefore essentially correct, which ensures an accurate estimate of the core-valence matrix elements appearing in the f sum rule.

Having determined $n_v^{\rm eff}(G)$, $\epsilon_{\mathbf{GG}}^v(0,\omega)$ appearing in the denominator of (2.36) was approximated by the electron gas dielectric function in which the Lindhard function is scaled by a factor $n_v^{\rm eff}(G)/n_v$. To calculate $\epsilon_{00}^v(\mathbf{q}\to\mathbf{0},\omega)$, however, a more accurate approximation is necessary. We propose using (2.28), in which the valence susceptibility is evaluated with band states determined by pseudopotential theory. This approach suggests itself since it was in fact designed to facilitate the calculation of valence states of nearly-free-electron metals. However, it should be borne in mind that although pseudopotential theory in principle yields the correct band energies, the wave functions obtained from the solution of the pseudopotential eigenvalue problem are not the true wave functions and will not in general yield correct matrix elements.

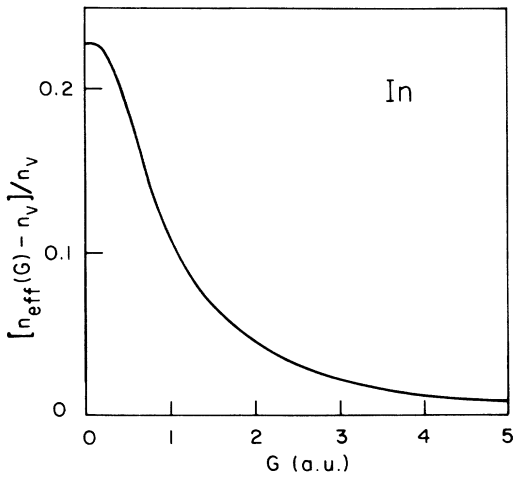

FIG. 2. Effective valence electron density of In as defined by the f sum rule, Eq. (4.1), vs wave vector in atomic units.

TABLE I. The change in f sum rule oscillator strength $[n_{\rm eff}(G)-n_v]/n_v$, as defined in (4.1) for valence electron transitions for some reciprocal lattice vectors **G**.

Cd		In		Sn		Hg		Al	
G	$\Delta n/n_v$	G	$\Delta n/n_v$	G	$\Delta n/n_v$	G	$\Delta n/n_v$	G	$\Delta n/n_v$
0.0	0.3544	0.0	0.2272	0.0	0.1894	0.0	0.4791	0.0	0.0487
1.30	0.0991	1.22	0.0878	1.21	0.0880	1.27	0.1253	1.42	0.0322
1.50	0.0805	1.41	0.0724	1.39	0.0742	1.47	0.1007	1.64	0.0287
2.13	0.0482	2.00	0.0428	1.97	0.0453	2.08	0.0585	2.33	0.0201
2.50	0.0378	2.34	0.0333	2.31	0.0353	2.44	0.0455	2.73	0.0162
2.61	0.0353	2.45	0.0311	2.41	0.0329	2.55	0.0423	2.85	0.0152
3.01	0.0274	2.83	0.0246	2.79	0.0261	2.94	0.0326	3.29	0.0119
3.28	0.0232	3.08	0.0212	3.04	0.0225	3.21	0.0274	3.59	0.0100
3.67	0.0220	3.16	0.0202	3.12	0.0215	3.29	0.0260	3.68	0.0095

The implication of this for calculations of the optical absorption of simple metals has been the subject of several investigations.[5–8] Valence interband transition matrix elements are found to be enhanced when orthogonalized plane waves (OPW's) are used instead of the plane-wave expanded pseudo-wave-functions. This enhancement effect can be included approximately without resorting to OPW's by scaling interband transition matrix elements by an appropriate factor in order that the f sum rule is fulfilled.

If the valence susceptibility is calculated using pseudo-wave-functions, the f sum rule yields the actual valence density n_v since the core electron degrees of freedom are eliminated by the pseudopotential transformation. Decomposing $\mathrm{Im}\chi_v^0(\mathbf{q},\mathbf{q},\omega)_{\rm pseudo}$ into intraband and interband parts, we obtain

$$\int_0^\infty \frac{d\omega}{\pi}\omega\,\mathrm{Im}\chi_v^0(\mathbf{q},\mathbf{q},\omega)_{\rm pseudo}=-\tfrac{1}{2}q^2 n_v = -\tfrac{1}{2}q^2\left[\frac{m}{m_{\rm opt}}n_v+n_{\rm IB}^{\rm pseudo}\right], \tag{4.8}$$

where the optical mass $m_{\rm opt}$ characterizes the intraband term and is given by[3]

$$m_{\rm opt}^{-1}=\frac{1}{4\pi^3 n_v}\sum_{n\in v}\int d^3k\, f_0(E_{n\mathbf{k}})\tfrac{1}{3}\nabla_{\mathbf{k}}^2 E_{n\mathbf{k}}\ . \tag{4.9}$$

Here the Fermi function $f_0(E_{n\mathbf{k}})$ ensures that only occupied valence states are included. Note that the intraband term involves only the band energies which are reproduced correctly by pseudopotential theory. The effective interband density $n_{\rm IB}^{\rm pseudo}$ follows from (4.8),

$$n_{\rm IB}^{\rm pseudo}=\left[1-\frac{m}{m_{\rm opt}}\right]n_v\ . \tag{4.10}$$

The sum rule for the true valence response function can also be separated into intraband and interband contributions $[n_v^{\rm eff}(0)=n_v+\Delta n]$:

$$\int_0^\infty \frac{d\omega}{\pi}\omega\,\mathrm{Im}\chi_v^0(\mathbf{q},\mathbf{q},\omega)=-\tfrac{1}{2}q^2(n_v+\Delta n) = -\tfrac{1}{2}q^2\left[\frac{m}{m_{\rm opt}}n_v+n_{\rm IB}\right]\ . \tag{4.11}$$

If we assume the band energies to be the same as in the pseudopotential theory, the intraband contribution and hence the optical mass is the same in both cases. The enhancement of the valence response due to the presence of the core states thus resides in the interband term. From (4.11) we have

$$n_{\rm IB}=\left[1-\frac{m}{m_{\rm opt}}\right]n_v+\Delta n\ . \tag{4.12}$$

Comparison of (4.12) with (4.10) shows that the interband oscillator strength is actually enhanced by the factor

$$\beta=n_{\rm IB}/n_{\rm IB}^{\rm pseudo}=1+\frac{\Delta n/n_v}{1-m/m_{\rm opt}}\ . \tag{4.13}$$

To a first approximation the pseudopotential theory result for (2.28) can be used provided the interband term is scaled by the factor β to account for the modified sum rule.

For polyvalent metals degenerate perturbation theory must be used to describe states near a gap at the Brillouin-zone boundaries. One obtains[25]

$$\mathrm{Im}[\epsilon_{00}^v(\omega)]_{\rm inter}=-\lim_{q\to 0}\frac{4\pi}{q^2}\mathrm{Im}[\chi_v^0(\mathbf{q},\mathbf{q},\omega)]_{\rm inter} =\tfrac{1}{3}\beta\sum_{\mathbf{G}}\frac{|2V_{\mathbf{G}}|^2E_G^2}{\omega^4}\frac{\mathrm{Im}\epsilon_L(G,\omega)}{[1-(2V_{\mathbf{G}}/\omega)^2]^{1/2}} \times\Theta(\omega-|2V_{\mathbf{G}}|)\ , \tag{4.14}$$

where $E_G=G^2/2$, $V_{\mathbf{G}}$ are the Fourier coefficients of the pseudopotential, and $\epsilon_L(G,\omega)$ is the well-known Lindhard dielectric function for an electron gas of density n_v. The factor β has been inserted to account for the enhancement discussed above.

The imaginary part of the intraband term, which is highly singular at zero frequency in the absence of any scattering, can be modeled by a Drude-like term to include the effects of scattering in a constant relaxation-time approximation. Taking into account the optical mass, we have

$$\mathrm{Im}[\epsilon_{00}^v(\omega)]_{\rm intra}=\omega_p^2\frac{m}{m_{\rm opt}}\frac{1/\tau}{\omega(\omega^2+1/\tau^2)}\approx\frac{m}{m_{\rm opt}}\frac{\omega_p^2}{\omega^3\tau} \tag{4.15}$$

for $\omega \gg \tau^{-1}$. τ can be estimated from the dc conductivity.

The real part of $\epsilon_{00}^{v}(\omega)$ follows by Kramers-Kronig, and using the f sum rule we obtain (again neglecting contributions of order τ^{-2})

$$\mathrm{Re}\epsilon_{00}^{v}(\omega)=1-\frac{\omega_p^{*2}}{\omega^2}+\tfrac{1}{3}\beta\sum_{\mathbf{G}}|2V_{\mathbf{G}}|^2E_G^2 I(G,\omega)/\omega^4 , \quad (4.16)$$

where

$$I(G,\omega)=P\int_{2|V_G|}^{\infty}\frac{d\omega'}{\pi}\left[\frac{1}{\omega'-\omega}+\frac{1}{\omega'+\omega}-\frac{2}{\omega'}\right] \times\frac{\mathrm{Im}\epsilon_L(G,\omega')}{[1-(2|V_G|/\omega')^2]^{1/2}} \quad (4.17)$$

and $\omega_p^{*2}=4\pi(n_v+\Delta n)$ is a free-electron plasma frequency corresponding to the effective valence electron density.

For large frequencies, $\omega \gg |2V_{\mathbf{G}}|$, (4.14) and (4.16) reduce to

$$\mathrm{Im}[\epsilon_{00}^{v}(\omega)]_{\mathrm{inter}}=\frac{\beta}{3}\sum_{\mathbf{G}}\frac{|2V_{\mathbf{G}}|^2E_G^2}{\omega^4}\mathrm{Im}\epsilon_L(G,\omega) \quad (4.18)$$

and

$$\mathrm{Re}\epsilon_{00}^{v}(\omega)=1-\frac{\omega_p^{*2}}{\omega^2}+\frac{\beta}{3}\sum_{\mathbf{G}}\frac{|2V_{\mathbf{G}}|^2E_G^2}{\omega^4}\mathrm{Re}[\epsilon_L(G,\omega)-\epsilon_L(G,0)] . \quad (4.19)$$

These are the expressions used in the calculations to represent the valence part of the dielectric function. They are valid for systems of cubic symmetry or as an angular average for anisotropic systems. To complete their specification we must also determine the parameter β, defined in (4.13), which involves the optical mass. This can be taken from experiment, but we have decided for consistency to calculate it using the expression which is correct to second order in the pseudopotential. These values are given in Table II. An additional reason for using the calculated optical masses is that we have taken all metals to be face centered cubic, whereas in reality In, Cd, Sn, and Hg are noncubic. The optical mass is sensitive to the geometry of the Fermi surface and the experimental value would therefore be inappropriate. However, it should be stressed that these approximations are only of secondary importance since the last term in (4.19) is relatively unimportant at and above the plasma frequency. Thus the real part of the valence dielectric function essentially takes the Drude form but with the enhanced plasma frequency ω_p^* replacing ω_p^0. ω_p^* is itself defined simply by the f-sum-rule enhanced valence density.

Equations (4.18) and (4.19) were evaluated using a local pseudopotential. The small-G pseudopotential form factors V_G are in many cases known from fits to experimental Fermi surface data but large G values of V_G are also required in the evaluation of (4.19). To obtain these we consider a Heine-Abarenkov model potential of the form

$$U(r)=\begin{cases}+\dfrac{Z}{R_c}u, & r<R_c\\ -\dfrac{Z}{r}, & r>R_c,\end{cases} \quad (4.20)$$

where R_c is the effective core radius and the constant Zu/R_c accounts for the repulsion arising from a d electron core.[26,27] For $u\to 0$, (4.20) reduces to an Ashcroft empty core local potential.

TABLE II. Metallic parameters used in the calculations: r_s is the electron density parameter, m_{opt}/m is the pseudopotential theory calculation of the optical to electron mass ratio, β is the enhancement factor defined in (4.13), and R_c and u are the Heine-Abarenkov model potential parameters, Eq. (4.20).

	r_s	m_{opt}/m	β	R_c (Å)	u
Cd	2.59	2.04	1.70	0.62[a]	0.35[a]
In	2.41	1.91	1.48	0.715[b]	0
Sn	2.22	1.93	1.39	0.53[c]	0.20[c]
Hg	2.65	2.87	1.74	0.47[d]	0
Al	2.07	1.52	1.14	0.60[e]	0

[a]Reference 30.
[b]Reference 29.
[c]Reference 31.
[d]Reference 32.
[e]Reference 28.

The values of the parameters R_c and u are given in Table II for the various metals considered. These were taken from the literature for Al (Ref. 28) and In,[29] but were obtained for Cd,[30] Sn,[31] and Hg (Ref. 32) by fitting to empirically derived pseudopotential form factors. The fit for Sn is quite good but less satisfactory for Hg. For Cd, a nonlocal pseudopotential is in principle required to fit the experimental Fermi surface so the values we have chosen should be thought of as providing a fit to only the local part. One should of course keep in mind that even in cases where the small-G form factors are rather well represented by a local model potential, there is very little information available to ascertain the accuracy of the large-G components. Nevertheless we expect our choice of parameters to provide a reasonable approximation to the pseudopotential form factors in the evaluation of (4.19) and some evidence for this will be given later. In any event, the smallness of the pseudopotential effects on the valence response at high frequencies diminishes the importance of any errors that we make.

The actual pseudopotential form factor V_G is a product of the Fourier transform of the atomic pseudopotentials U_G screened by $\epsilon_L(G,0)$ and the appropriate (normalized) geometric structure factor S_G. As mentioned previously, only Al of all the metals considered is fcc, however we have for simplicity assumed all to have the same close-packed structure. Such an approximation is clearly inappropriate in discussions of the Fermi surface but should be useful in obtaining the average dielectric func-

tion of the metal. We anticipate the anisotropy of the dielectric function of the metals studied to be relatively weak.

V. RESULTS AND DISCUSSION

A. Cd, In, and Sn

We begin with a discussion of the dielectric properties of the metals Cd ($Z=48$), In ($Z=49$), and Sn ($Z=50$). These neighboring elements in the periodic table have $4d$ thresholds as determined in the self-consistent DFT calculations of 9.9, 15.8, and 22.8 eV, respectively, which are about an electronvolt lower in energy than those observed.[33] As discussed in Sec. III, the difference between the theoretical and experimental threshold energies is a limitation of the LDA and not of the single-cell approximation used in the electronic-structure calculations.

Our results for the dielectric function are based on Eq. (2.36). Figure 3 illustrates the behavior of ϵ_2 in the vicinity of the $4d$ threshold of Cd. In this region the CM term in (2.36) dominates, and it can be seen that the core excitations give rise to a peak with a distinctive asymmetric profile. The absorption is essentially atomiclike but is modified strongly by the local fields in the solid. This point is illustrated in Fig. 3, which also shows the imaginary part of the core polarizability, $\mathrm{Im}\alpha(\omega)$, multiplied by $4\pi n_i$. This quantity represents the dielectric function of a set of independent polarizable ions and the enhancement of ϵ_2 above this level is a consequence of the local fields. Furthermore, in contrast to the core polarizability, the CM term exhibits absorption below threshold as a result of valence electron excitations induced by the dipolar fields of the cores. This can be seen more clearly by writing the CM term in the following form:

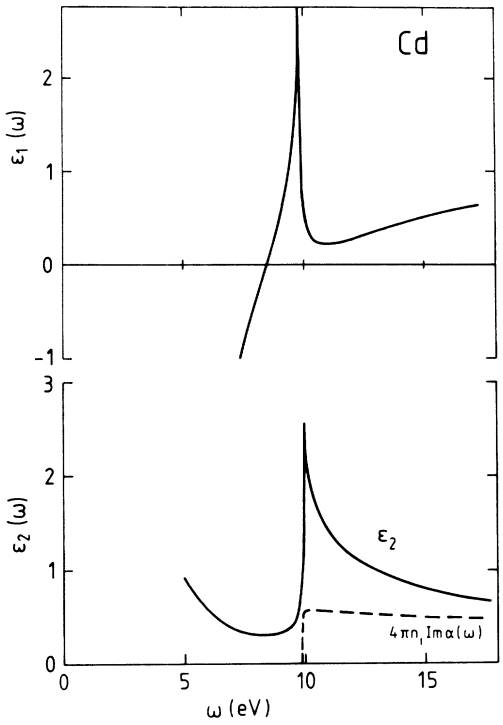

FIG. 3. Real (ϵ_1) and imaginary (ϵ_2) parts of the dielectric function of cadmium in the vicinity of the $4d$ threshold. The dashed curve indicates the ionic contribution to $\epsilon_2(\omega)$ in the absence of local field effects.

$$\mathrm{Im}\epsilon_{\mathrm{CM}} \simeq \tfrac{1}{3}[\mathrm{Re}\epsilon_{\mathrm{CM}}(\omega)]^2 \sum_{G\neq 0} f(\mathbf{G},\omega)\mathrm{Im}[-1/\epsilon_L(G,\omega)] \tag{5.1}$$

with

$$\mathrm{Re}\epsilon_{\mathrm{CM}} \simeq \frac{4\pi n_i \alpha(\omega)}{1-\frac{4\pi}{3}n_i\alpha(\omega)\left[1+\sum_{G\neq 0} f(G,\omega)\left[1-\mathrm{Re}\frac{1}{\epsilon_L(G,\omega)}\right]\right]}, \tag{5.2}$$

which is a good approximation when the imaginary part is small. Equation (5.1) shows that the absorption below threshold is due to excitation of the valence electrons [$\alpha(\omega)$ and hence $f(G,\omega)$ are real] and adds to the interband absorption given by (4.14). (The Drude intraband absorption is negligibly small for high frequencies at low temperature.) We note that the dipole form factor appears linearly in (5.1) rather than quadratically, as would occur for a dipolar external field applied directly to the valence electrons. The difference is due to the fact that the excitation of valence electrons as described by the CM term is due to the indirect coupling of the valence electrons to the external field via the polarizable cores.

Figure 4 illustrates the frequency dependence of the various contributions to $\epsilon_2(\omega)$ for In. We observe that $\mathrm{Im}\epsilon_{\mathrm{CM}}(\omega)$, (5.1), and $\mathrm{Im}\epsilon_{\mathrm{inter}}(\omega)$, (4.18), are of equal importance close to the plasma frequency (see below). The relative magnitude of the various Fourier components contributing to (5.1) is dictated by the dipolar form factors. These are shown as a function of G for a few frequencies in Fig. 5 in the case of In. The extent of the form factor in reciprocal space is roughly inversely proportional to the core radius.

As the threshold energy is approached from below, the real part of the polarizability increases due to the logarithmic singularity illustrated in Fig. 1. The magnitude of the denominator in the CM term therefore decreases leading to the large enhancement of $\mathrm{Im}\epsilon_{\mathrm{CM}}(\omega)$ just below threshold. This enhancement persists through the threshold as $\mathrm{Im}\alpha(\omega)$ switchs on, but as the frequency continues to increase, $\mathrm{Re}\alpha(\omega)$ rapidly decreases and the enhancement diminishes in magnitude. This accounts for the sharp threshold behavior shown in Figs. 3, 6, and 7 for Cd, In, and Sn, respectively. This feature, however, is

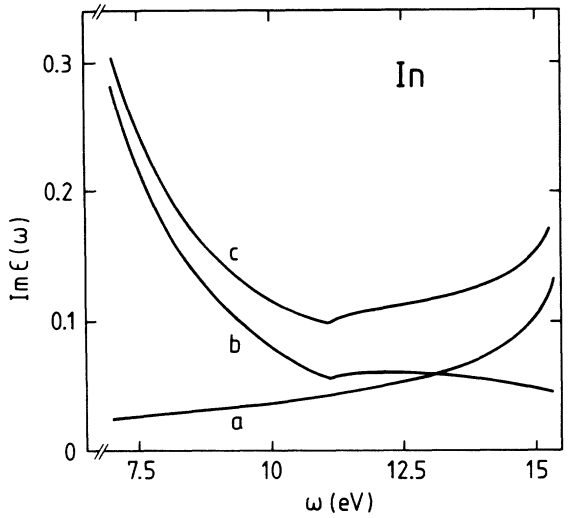

FIG. 4. Decomposition of $\epsilon_2(\omega)$ for In: b is the interband contribution calculated from (4.18); a is the local field effect calculated from (5.1); c is the sum of a and b.

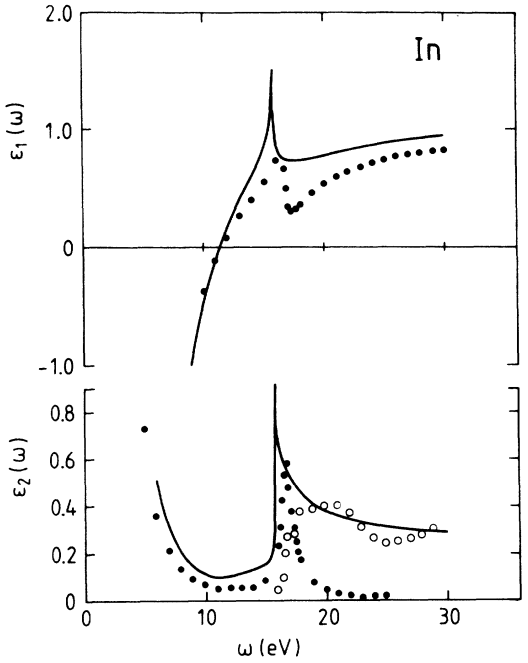

FIG. 6. Dielectric function of In vs frequency, in eV. The solid line is theory; the points are experimental values (solid circles, Ref. 37; open circles, Ref. 38).

partly an artifact of the approximations used to calculate the dielectric function. First, we have neglected the finite bandwidth of the $4d$ core band; the actual bandwidth of 1.69 eV (Ref. 34) will lead to a broadening of the threshold behavior. Second, one should also take into account the spin-orbit splitting of the atomic $4d$ level, which is about 1 eV.[35] Both of these effects will tend to eliminate the narrow, relatively weak threshold peak, but one would still expect to find a local field enhancement of ϵ_2 within a few electronvolts of threshold. ϵ_1 also has a sharp peak at the $4d$ threshold which is again associated with the singular behavior of $\mathrm{Re}\alpha(\omega)$. The sudden onset of $\mathrm{Im}\alpha(\omega)$ above threshold in turn causes ϵ_1 to decrease rapidly to a minimum beyond which it recovers towards unity.

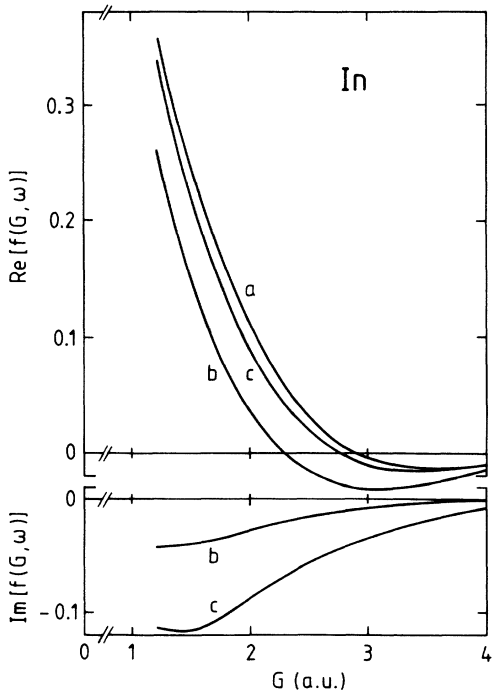

FIG. 5. Real and imaginary parts of the dipole form factor $f(G,\omega)$ vs wave vector for various frequencies: curve a, $\omega=5$ eV; curve b, $\omega=16$ eV; curve c, $\omega=24$ eV.

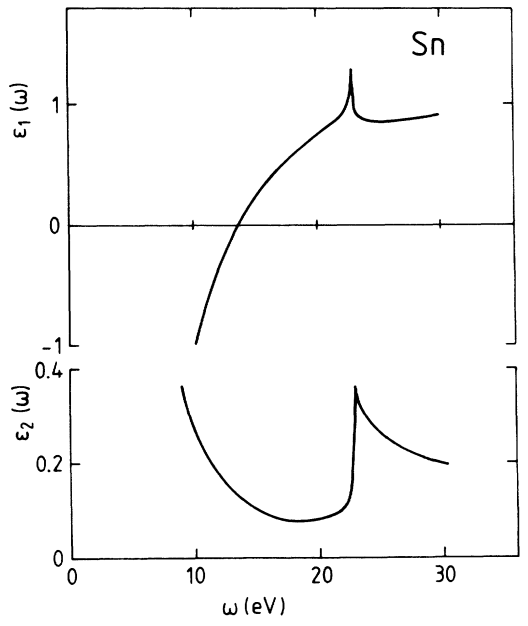

FIG. 7. Dielectric function of Sn vs frequency, in eV.

The zero crossing of ϵ_1 at 8.5 eV in Fig. 3 is the signature of the collective plasmon mode. According to (2.36) and (4.19) there are two sources which contribute to a possible shift of the plasma frequency from its free-electron value ω_p^0. Since the last term in (4.19) is found to be a small correction at the plasma frequency, the valence dielectric function by itself yields a plasma frequency equal to the *enhanced* value ω_p^* defined after (4.17). These values are presented in Table III, where it can be seen that the effect of the f sum-rule enhancement of the valence electron density is to increase the frequency by as much as 2 eV above ω_p^0. Yet the observed plasma frequency is actually below the free-electron value. The theoretical value as obtained from (2.36) is

$$\omega_p = \frac{\omega_p^*}{[1+\mathrm{Re}\epsilon_{\mathrm{CM}}(\omega_p)]^{1/2}} . \tag{5.3}$$

The term $\mathrm{Re}\epsilon_{\mathrm{CM}}(\omega)$ accounts for core polarization and local-field effects and leads to a reduction of the plasma frequency by an amount which more than compensates for the upward shift from ω_p^*. The final small shift of ω_p due to the last term in (4.19) can be treated perturbatively yielding

$$\Delta\omega_p = -\frac{\mathrm{Re}\epsilon_{\mathrm{inter}}^{v}(\omega_p)}{\frac{2\omega_p^{*2}}{\omega_p^3}+\left[\frac{\partial\,\mathrm{Re}\epsilon_{\mathrm{CM}}}{\partial\omega}\right]_{\omega=\omega_p}} \tag{5.4}$$

with ω_p determined by (5.3). All these effects are included in the final numerical results shown in Table III. The overall good agreement with the experimental values cannot be achieved without taking into account the competing effects of f sum-rule enhancement and core polarization. The simple addition of an ionic dielectric constant to represent the polarizable ions is too naive an approximation and fundamentally incomplete.

The finite value of ϵ_2 at ω_p is due to valence intersubband transitions and core-polarization-induced valence excitations. This gives the plasmon a width (Δ_{FWHM}) which for a well-defined mode is given by the expression

$$\Delta_{\mathrm{FWHM}} = 2\left[\mathrm{Im}\epsilon_{\mathrm{inter}}^{v}+\mathrm{Im}\epsilon_{\mathrm{CM}}\right]\cdot\left|\frac{\partial\,\mathrm{Re}\epsilon(\omega)}{\partial\omega}\right|_{\omega=\omega_p}^{-1} . \tag{5.5}$$

In Fig. 8 we show the energy-loss function for Cd. The plasmon peak has a width of about 0.7 eV, which compares favorably with that determined from experiment.[27,36] The broad shoulder above the plasmon peak is due to 4d electron excitations and is discernable in some of the experimental energy loss functions.[27,36] The energy-loss functions of In and Sn shown in Figs. 9 and 10 are similar.

Our calculations also allow us to comment on the surface-plasmon frequency which is given by

$$\mathrm{Re}\epsilon_M(\omega)+1=0 . \tag{5.6}$$

TABLE III. Bulk and surface plasma frequencies (eV): free electron (ω_p^0,ω_{sp}^0), valence (ω_p^*), and theoretical and experimental (ω_p,ω_{sp}).

	ω_p				ω_{sp}		
	ω_p^0	ω_p^*	Theor.	Expt.	ω_{sp}^0	Theor.	Expt.
Al	15.8	16.2	15.6	14.92[a] 15.3[b]	11.2	11.2	10.6[b]
Ag	9.0[c]			3.76[d] 3.78[e]	6.35[c]		3.63[d]
Cd	11.3	13.2	8.5	9.25[f] 9.07[g] 9.4[h] 9.2[i]	8.0	7.4	7.30[f]
In	12.6	14.0	11.3	11.3[j] 11.4[b,h,i]	8.9	8.9	8.7[b,j]
Sn	14.2	15.5	13.7	14.1[j] 13.76[k] 13.85[l]	10.0	10.1	10.4[j] 9.7[l]
Sb	15.1			15.3[m]	10.7		10.85[m]
Hg	10.9	13.3	8.0	7.3[n]	7.7	7.2	6.2[n] 6.35[o] 6.3[p]

[a]Reference 45.
[b]Reference 46.
[c]Using $r_s=3.01$.
[d]Reference 47.
[e]Reference 48.
[f]Reference 49.
[g]Reference 27.
[h]Reference 36.
[i]Reference 50.
[j]Reference 51.
[k]Reference 52.
[l]Reference 53.
[m]Reference 54.
[n]Reference 41.
[o]Reference 55.
[p]Reference 56.

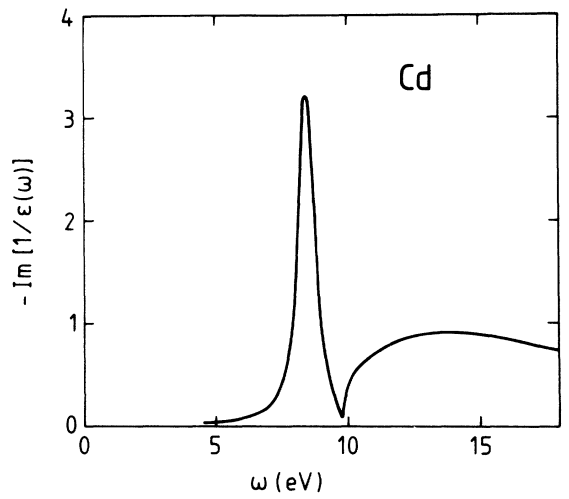

FIG. 8. Energy-loss function of Cd vs frequency, in eV.

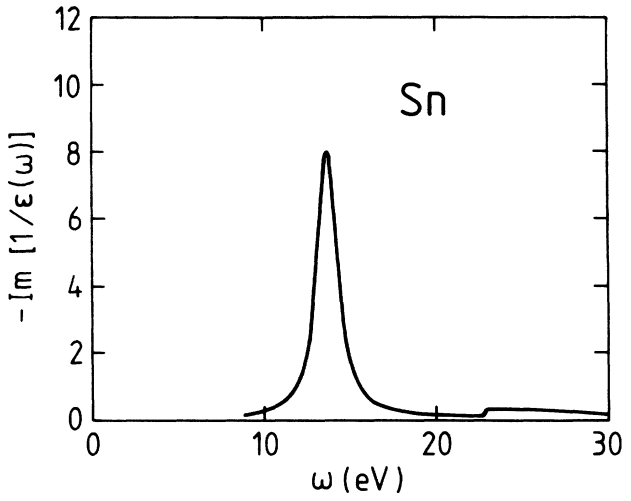

FIG. 10. As in Fig. 8, but for Sn.

For free electrons this leads to the well-known result $\omega_{sp}^0=\omega_p^0/\sqrt{2}$ which relates ω_{sp}^0 and ω_p^0 in a simple way. The situation in reality is more complex. Neglecting once again interband transitions [the last term in (4.19)], ω_{sp} is determined by

$$\omega_{sp}=\frac{\omega_p^*}{[2+\mathrm{Re}\epsilon_{\mathrm{CM}}(\omega_{sp})]^{1/2}} \tag{5.7}$$

so that

$$\frac{\omega_p}{\omega_{sp}}=\left[\frac{2+\mathrm{Re}\epsilon_{\mathrm{CM}}(\omega_{sp})}{1+\mathrm{Re}\epsilon_{\mathrm{CM}}(\omega_p)}\right]^{1/2}. \tag{5.8}$$

As the magnitude of the CM dielectric function increases, this ratio diminishes. The numerical results for this quantity are compared with experimental values in Fig. 11, which also includes Ag and Sb to illustrate the systematic trend with position of the $4d$ band. The trend is clearly associated with the proximity of the $4d$-band excitation threshold to the plasma frequency.

We now turn to a more-detailed comparison of the calculated dielectric function of In with available experimental data. Some of these results (Fig. 6) were presented previously,[1] however the present work incorporates an improved estimate of interband excitations. The solid points in Fig. 6 are the data of Krane[37] and are derived from a Kramers-Kronig analysis of the electron-energy-loss spectrum as measured over a limited range of energies. The open circles are taken from the optical conductivity ($\sigma_1=\omega\epsilon_2/4\pi$) data of Jezequel *et al.*[38] The two sets of data are only in qualitative agreement in that ϵ_2 of Krane exhibits a peak at threshold and then drops off rapidly with increasing frequency while the optical conductivity data show a rather constant absorption above threshold up to 30 eV. Although the theoretical calculation has a sharp peak at threshold, it does not contain much intensity and should be broadened for the reasons given above. The theory therefore appears to be in better

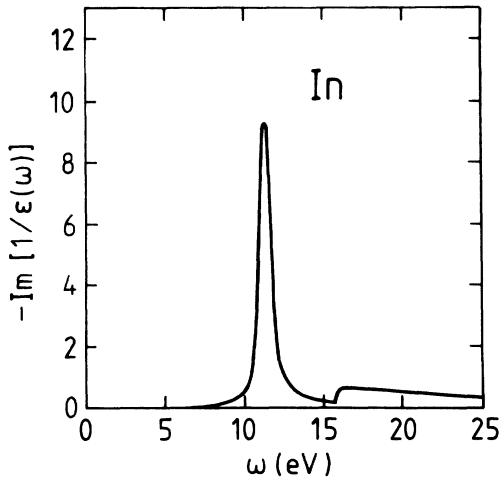

FIG. 9. As in Fig. 8, but for In.

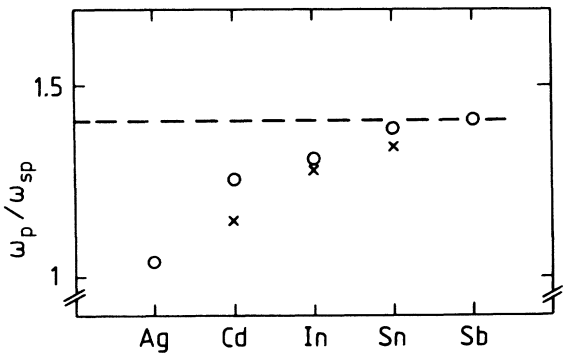

FIG. 11. Ratio of bulk-to-surface plasmon frequencies. The open circles are experimental values and the crosses are theory. The dashed line is the free-electron value.

overall agreement with the data of Jezequel *et al.*[38] The general shape of ϵ_1 in Krane's data[37] is consistent with the calculated behavior at threshold but the minimum is more pronounced, probably because of the narrower structure in ϵ_2.

A further comparison with experiment is available in measurements of the absorption coefficient $\mu=\omega\epsilon_2/nc$ made by Lemonnier[39] and by Leveque *et al.*[40] Here, n is the refractive index. Lemonnier's data, reproduced in Fig. 12 together with the theoretical results, show a peak centered at 22 eV followed by a minimum at 27 eV, and appears not to be consistent with those of Krane[37] but is similar to those of Jezequel *et al.*[38] In view of the variability of the measurements over this frequency range, more-reliable data are obviously necessary to provide a definitive comparison with theory. For now we can claim only qualitative agreement with the data in the vicinity of the 4*d* excitation threshold.

Leveque *et al.*[40] give the absorption coefficient over a more extended range of frequencies from 40 to 220 eV, which is compared with theory in Fig. 13. In this range of frequencies the absorption observed is essentially the 4*d* absorption of the free atom with relatively small solid-state corrections. The broad peak centered at about 70 eV is due to the excitation of 4*d* electrons to final *f* states and constitutes the giant dipole resonance exhibited by elements in this part of the periodic table. The good agreement found in our calculation is consistent with the successful application of time-dependent density-functional theory to the calculation of atomic photoabsorption.[14] When viewed over this broader range of frequencies, it becomes clear that the threshold behavior of the 4*d* interband excitations is characteristic of the solid and not that of the free atom. The threshold behavior therefore serves as a sensitive probe of the dielectric function and a test of the approximations used in its evaluation.

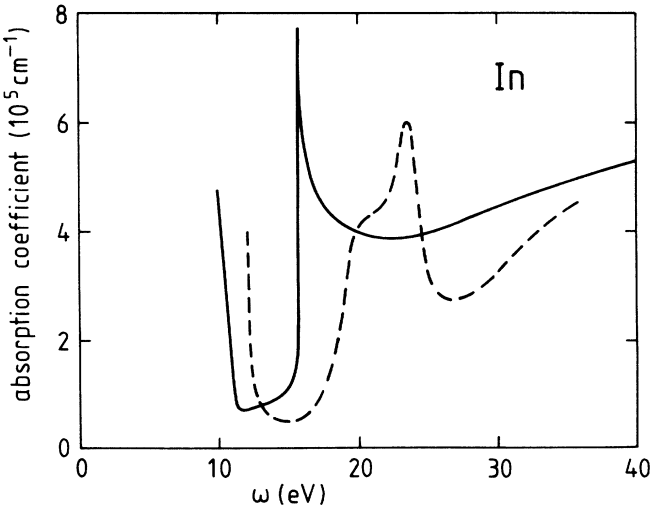

FIG. 12. The absorption coefficient $\mu=\omega\epsilon_2/nc$ of In vs frequency. The solid line is theory and the dashed curve is the experimental data of Lemonnier, Ref. 39.

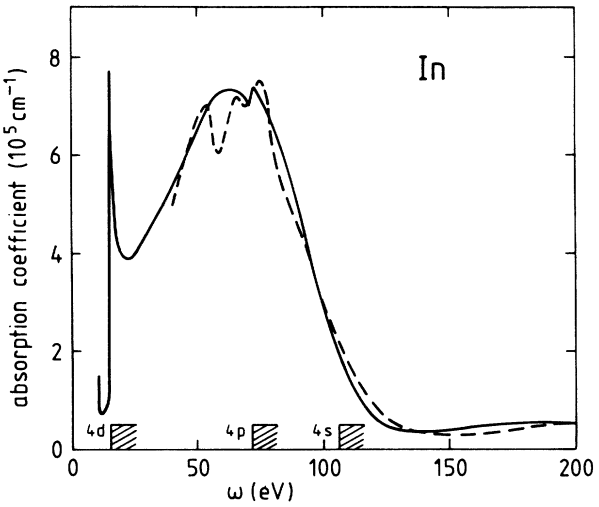

FIG. 13. The absorption coefficient of In over an extended frequency range. The solid line is theory and the dashed line is the experimental data of Leveque *et al.*, Ref. 40. The dashed areas along the abscissa indicate the theoretical core excitation thresholds.

B. Hg

The results for mercury are qualitatively similar to those for the previous three metals, particularly Cd, and are summarized in Figs. 14 and 15. The theoretical plasma frequency is reduced from $\omega_p^0=10.9$ eV to 8 eV and compares favorably with the experimental value of 7 eV which has been determined using optical techniques.[41]

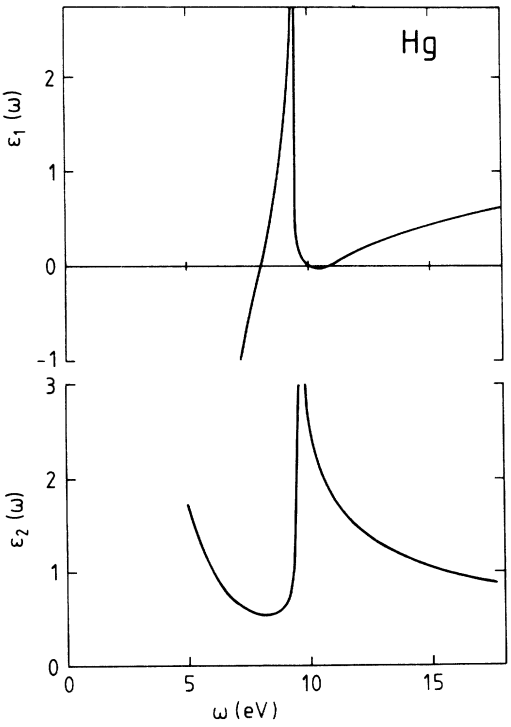

FIG. 14. As in Fig. 7, but for Hg.

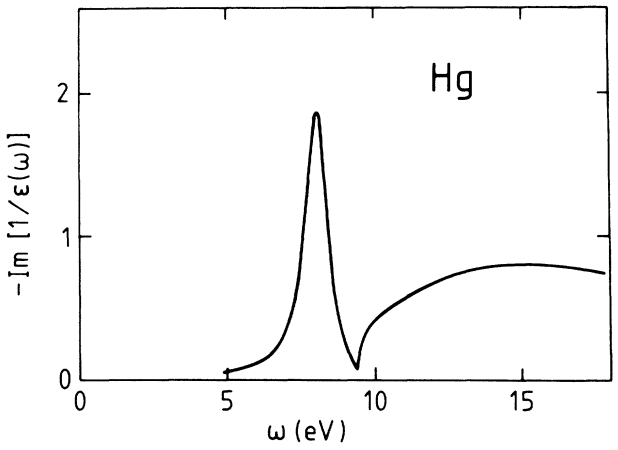

FIG. 15. As in Fig. 8, but for Hg.

Like Cd, the 5*d* core level is very close to the conduction band and has an excitation threshold of 9.5 eV [cf. the experimental value (Ref. 33) of 7.7–9.5 eV]; core excitations contribute significantly to the energy-loss function above 10 eV as shown in Fig. 15.

C. Al

Aluminum is a prototypal simple metal in which core polarization effects are not expected to be of much importance since the 2*p* core states are tightly bound and hence weakly polarizable. Nevertheless, the free-electron plasma frequency for this metal is 15.8 eV, which differs by a surprisingly large amount from the experimental value of 15.0 eV. The discrepancy has previously been attributed[25] to a combination of band-structure and core-polarization effects. The latter are accurately treated in the present work while the former are included by means of pseudopotential theory with the scaling modification required for consistency with the *f* sum rule. We have carried out calculations for this simple metal in order to quantify the importance of core polarization, thereby establishing the magnitude of the plasma frequency shift which must be attributed to other sources.

We find that the core enhancement of the valence *f* sum rule is approximately 5%, which gives $\omega_p^* = 16.2$ eV. The inclusion of core polarization then reduces the plasma frequency back to a value of 16.0 eV, which is still higher than the original free-electron value of 15.8 eV. Thus, although core polarization moves the plasma frequency in the direction expected, it is a relatively weak effect as compared to the situation for Cd or In and is not sufficient to compensate for the correction from the *f* sum rule. An additional shift of approximately −0.4 eV arises from the last term in (4.19) and brings the final theoretical value to 15.6 eV (Table III). This still falls short of the experimental plasma frequency of about 15 eV. As a partial explanation of this discrepancy, one can observe in Fig. 17 that the values of $\epsilon_2(\omega)$ calculated from (4.18) lie below the measured values in the region above the plasma frequency. Stronger interband absorption above ω_p would necessarily result, via a Kramers-Kronig analysis, in an increased downward shift of the plasma frequency and would bring theory and experiment into better agreement. However, a more detailed calculation of the valence dielectric function than that carried out in Sec. IV is obviously required in order to establish the degree of improvement. As a final comment, we have tacitly assumed that the RPA provides an accurate description of the nonlocal response of a crystalline material; the extent to which this supposition is valid is not known.

A more direct test of our description of core polarization in Al is provided by measurements of the dielectric function in the vicinity of the *L*-shell threshold, which is found experimentally at 72 eV. The calculated core polarizability is shown on a semilogarithmic scale in Fig. 16. The 2*p* edge is found at 64 eV, where $\mathrm{Im}\alpha(\omega)$ is discontinuous and $\mathrm{Re}\alpha(\omega)$ has a logarithmic singularity. Both of these features persist in the real and imaginary parts of ϵ, which are shown in Fig. 17 with the experimental results.[42] Above threshold, the calculated ϵ_2 is in good agreement with experiment apart from the observed fine structure, which presumably is a consequence of final-state scattering from neighboring atoms in the crystal. ϵ_1 is likewise in good qualitative agreement, although the calculated value just above threshold is somewhat smaller than experiment. Both theory and experiment show the distinctive edge singularity which has its origin in the core polarizability $\alpha(\omega)$; in fact, the deviation of ϵ_1 from unity is seen to follow closely the frequency dependence of $\alpha(\omega)$ shown in Fig. 16. However, an interesting difference showing the effect of the denominator in the CM term occurs just above threshold where $\mathrm{Re}\alpha(\omega)$ has a shoulder while ϵ_1 acquires a rounded peak.

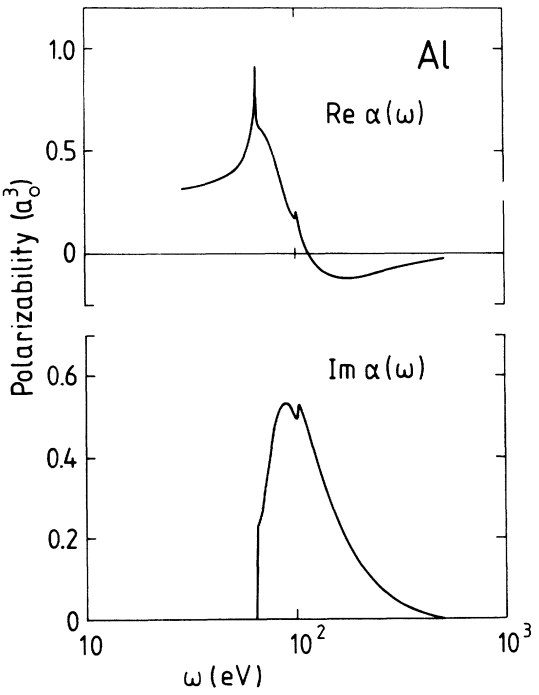

FIG. 16. Core polarizability $\alpha(\omega)$ of Al on a logarithmic frequency scale.

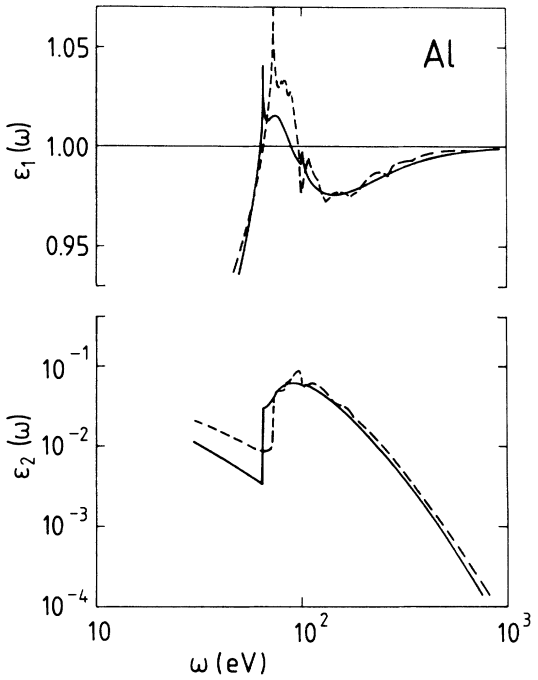

FIG. 17. Dielectric function of Al in the vicinity of the L-shell threshold. The solid line is theory and the dashed line is the experimental result, Ref. 42.

VI. CONCLUSIONS

In this paper we have studied the dielectric function of simple metals with shallow core states in a range of frequencies where the dynamical response of both valence and core electrons contribute with equal importance. Since the extended valence electrons and localized core electrons respond quite differently to an externally applied potential, appropriate partial response functions for the two subsystems were defined and calculated using suitable approximations. The response of the core electrons can be accounted for by a local atomic core polarizability $\alpha(\omega)$, which differs from that of a free atom or ion due to the fact that the core resides in a metallic environment. The response of the extended states is described in terms of a valence dielectric function $\underline{\epsilon}^v(\mathbf{q},\omega)$, which is calculated using a weak (local) pseudopotential treated to second order in perturbation theory. The macroscopic dielectric function of the combined core-valence system was then derived in terms of $\alpha(\omega)$ and $\underline{\epsilon}^v(\mathbf{q},\omega)$ by treating the Coulomb interaction between the lattice of core dipoles and the valence electron gas self-consistently.

As a characteristic feature of the solid state, $\alpha(\omega)$ exhibits in its real part a logarithmic singularly at the core threshold ω_T due to the presence of a sharp Fermi surface. This behavior is quite different from that of the Lorentz oscillator model used previously,[17] in which the continuous excitation spectrum above ω_T is compressed into a single line at ω_T. The lattice of core dipoles gives rise to a Clausius-Mossotti form of the core dielectric function with an important correction factor, which results from density fluctuations in the valence system induced by the local fields of the dipole lattice. The summation over reciprocal-lattice vectors in this correction factor is cut off by a dipole form factor $f(G,\omega)$, which drops off to a small value for $G \geq G_{\max} \sim R_c^{-1}$, accounting in this way for the finite extent of the core with the ionic radius R_c. This is an important modification to the point dipole model in which $f(G,\omega)=1$ for all G. The local field effects arising from the mutual interaction of the core and valence electrons give a sizeable contribution to $\mathrm{Im}\epsilon(\omega)$ *below* ω_T and enhance the effect of the core polarization close to ω_T.

The existence of core states is reflected in the valence electron f sum rule as an enhancement of the valence interband transition oscillator strength. This is ultimately related to the orthogonality of the core and valence states, which, for example, is explicitly taken into account in the OPW approximation. Here this effect has been taken into account approximately by rescaling the pseudopotential interband matrix element by an enhancement factor β derived from the required fulfillment of the total f sum rule. The core enhanced f sum rule valence density provides an important shift of the plasma frequency to a value above the free electron estimate ω_p^0.

Application of the present theory to plasmons and high-frequency optical properties offered a testing ground of the calculated dielectric function. The explicit inclusion of the core degrees of freedom leads to considerably improved agreement between theory and experiment for plasmon and surface-plasmon frequencies for metals with shallow core states. Calculated absorption spectra at higher frequencies, such as in the case of In and Al, provide a more direct test of the calculated core polarizability, and the good agreement with the experimental data confirms the accuracy of this atomic response property.

Some of the discrepancies we find are due to the neglect of the finite bandwidth of the d-electron core band and of spin-orbit interactions which lead to additional energy-level splittings. These approximations mainly affect details of the spectral distributions near threshold but should not significantly alter the weight of the distributed oscillator strengths of the calculated core polarizability. Our method does allow for the inclusion of local field effects whose importance has been demonstrated over an extended frequency range from below to well above threshold. Neglecting this effect can lead to quantitative differences. For example, the recent LMTO calculation of $\epsilon(\omega)$ of Cd,[27,43] in which local field effects are not included, yields a plasmon line which is considerably narrower than in our calculations.

There are also limitations in the use of a local pseudopotential in the calculation of the valence part of $\epsilon(\omega)$, particularly at high frequencies. Even if a local pseudopotential were to hold at these frequencies, the large-G Fourier components become important too, and these can only be estimated by a smooth extrapolation of the local model potential results. Reference to Fig. 17, for example, shows that an Ashcroft empty core potential underestimates the interband contribution to $\mathrm{Im}\epsilon(\omega)$ for $\omega_p < \omega < \omega_T$. However, the uncertainties connected with

the pseudopotential should not affect our qualitative conclusions regarding the importance of core polarization effects. Another concern is the truncation of the valence dielectric matrix to its diagonal elements, as in (2.35), which permits the simplification of (2.34) to the final form used in (2.36). The smallness of these local field effects was demonstrated in Ref. 25 within the nearly-free-electron approximation for simple metals and was contrasted with their importance for semiconductors.

The main advantage of the present formulation of the problem is that it admits a detailed and transparent discussion of the physical effects associated with the dynamical response of the core electrons. The theory presented here can also be extended to the finite-**q** dependence of the dielectric function, which would be necessary to investigate plasmon dispersion. This is interesting since In unexpectedly exhibits a stronger plasmon dispersion than Al, which suggests a dependence on core polarization. Our method should also allow a more-accurate estimate of the contribution of dispersion forces to the binding energy of metals,[9,10] which has recently attracted renewed interest.[44] We hope to address these problems in the future.

ACKNOWLEDGMENTS

This work was partially supported by a grant from the Natural Sciences and Engineering Research Council of Canada.

[1]E. Zaremba and K. Sturm, Phys. Rev. Lett. **55**, 750 (1985).
[2]C. Kunz, Z. Phys. **196**, 311 (1966).
[3]D. Pines, *Elementary Excitations in Solids* (Benjamin, New York, 1964).
[4]V. Heine, M. L. Cohen, and D. Weaire, *Solid State Physics: Advances in Research and Applications,* edited by H. Ehrenreich, F. Seitz, and D. Turnbull (Academic, New York, 1970), Vol. 24.
[5]J. A. Appelbaum, Phys. Rev. **144**, 435 (1966).
[6]A. O. E. Animalu, Phys. Rev. **163**, 557 (1967); **163**, 562 (1967).
[7]L. W. Beeferman and H. Ehrenreich, Phys. Rev. B **2**, 364 (1970).
[8]B. I. Bennet and S. H. Vosko, Phys. Rev. B **6**, 2119 (1972).
[9]J. J. Rehr, E. Zaremba, and W. Kohn, Phys. Rev. B **12**, 2062 (1975).
[10]K. K. Mon, N. W. Ashcroft, and G. V. Chester, Phys. Rev. B **19**, 5103 (1979).
[11]L. Hedin, Ark. Fys. **30**, 231 (1965). A somewhat different formulation is given in W. Hanke, Adv. Phys. **27**, 287 (1978).
[12]S. L. Adler, Phys. Rev. **126**, 413 (1962).
[13]N. Wiser, Phys. Rev. **129**, 62 (1963).
[14]A. Zangwill and P. Soven, Phys. Rev. A **21**, 1561 (1980).
[15]P. Hohenberg and W. Kohn, Phys. Rev. B **136**, 964 (1964).
[16]W. Kohn and L. J. Sham, Phys. Rev. A **140**, 1133 (1965).
[17]K. Sturm, Solid State Commun. **48**, 29 (1983).
[18]M. J. Stott and E. Zaremba, Phys. Rev. A **21**, 12 (1980); **22**, 2293 (1980).
[19]V. L. Moruzzi, J. F. Janak, and A. R. Williams, *Calculated Electronic Properties of Metals* (Pergamon, New York, 1978).
[20]L. Dagens, J. Phys. C **5**, 2333 (1972).
[21]C.-O. Almbladh and U. von Barth, Phys. Rev. B **13**, 3307 (1976); C.-O. Almbladh, U. von Barth, Z. D. Popovic, and M. J. Stott, *ibid.* **14**, 2250 (1976); E. Zaremba, L. M. Sander, H. B. Shore, and J. H. Rose, J. Phys. F **7**, 1763 (1977).
[22]G. W. Bryant and G. D. Mahan, Phys. Rev. B **17**, 1744 (1978); E. Zaremba and D. Zobin, Phys. Rev. Lett. **44**, 175 (1980); R. M. Nieminen and M. J. Puska, Phys. Rev. B **25**, 67 (1982).
[23]O. Gunnarsson and B. I. Lundqvist, Phys. Rev. B **13**, 4274 (1976).
[24]R. M. Nieminen and M. J. Puska, Phys. Scr. **25**, 952 (1982).
[25]K. Sturm, Adv. Phys. **31**, 1 (1982).
[26]See the discussion on p. 63 of Ref. 4.
[27]V. D. Gorobchenko, M. V. Zharnikov, E. G. Maksimov, and S. N. Rashkeev, Zh. Eksp. Teor. Fiz. **88**, 677 (1985) [Sov. Phys.—JETP **61**, 398 (1985)]. These authors used a model potential of this form for Cd but unfortunately they did not present the numerical values of R_c and u.
[28]N. W. Ashcroft and W. E. Lawrence, Phys. Rev. **175**, 938 (1968). Two possible choices for R_c are derived from fitting the Fermi surface. We prefer $R_c=0.715$ Å to $R_c=0.575$ Å since it gives an optical mass in better agreement with experiment.
[29]See p. 186 of Ref. 4. We used $R_c=0.60$ Å instead of 0.59 Å to fit V_{200} as closely as possible.
[20]R. W. Stark and L. M. Falicov, Phys. Rev. Lett. **19**, 795 (1967).
[31]J. E. Craven, Phys. Rev. **182**, 693 (1969).
[32]G. B. Brandt and J. A. Rayne, Phys. Rev. **148**, 644 (1966).
[33]See the Appendix in *Photoemission in Solids II,* Vol. 27 of *Topics in Applied Physics,* edited by L. Ley and M. Cardona (Springer-Verlag, Berlin, 1979).
[34]R. T. Poole, P. C. Kemeny, J. Liesegang, J. G. Jenkin, and R. C. G. Lecky, J. Phys. F **3**, L46 (1973). The bandwidth of 1.69 eV as determined by photoelectron spectroscopy is in good agreement with 1.5 eV obtained from band-structure calculations, Ref. 19.
[35]L. A. Hisscott and P. T. Andrews, J. Phys. F **5**, 1077 (1975).
[36]T. Aiyama and K. Yada, J. Phys. Soc. Jpn. **38**, 1357 (1975).
[37]K. J. Krane, J. Phys. F **8**, 2133 (1978) and Diploma Thesis, University of Hamburg, 1977 (unpublished).
[38]G. Jézéquel, J. Thomas, and J. C. Lemonnier, Solid State Commun. **23**, 559 (1977).
[39]J. C. Lemonnier, thèse Rennes, 1977 (unpublished).
[40]G. Leveque, C. G. Olson, and D. W. Lynch, Solid State Commun. **51**, 377 (1984).
[41]W. J. Choyke, S. H. Vosko, and T. W. O'Keeffe, Solid State Commun. **9**, 361 (1971).
[42]Physics Data: *Optical Properties of Metals,* edited by J. H. Weaver, C. Krafka, D. W. Lynch, and E. E. Koch (Fachinformationszentrum, Karlsruhe, 1981).
[43]E. G. Maksimov, I. I. Mazin, S. N. Rashkeev, and Yu A. Uspenski, J. Phys. F **18**, 833 (1988).
[44]A. C. Maggs and N. W. Ashcroft, Phys. Rev. Lett. **59**, 113 (1987).
[45]C. v. Festenberg, Z. Phys. **207**, 47 (1967).
[46]H. Raether, *Excitations of Plasmons and Interband Transitions by Electrons* (Springer-Verlag, Berlin, 1980).
[47]H. J. Hagemann, W. Gudat, and C. Kunz, J. Opt. Soc. Am. **65**, 742 (1975).
[48]J. Daniels, Z. Phys. **203**, 235 (1967).

[49]S. A. Abo-Namous, P. T. Andrews, and C. E. Johnson, J. Phys. F **9**, 61 (1979).
[50]T. Bornemann, J. Eickmans, and A. Otto, Solid State Commun. **65**, 381 (1988).
[51]J. L. Robins, Proc. Phys. Soc. **79**, 119 (1962).
[52]P. Zacharias, Z. Phys. **256**, 92 (1972).
[53]G. Jézéquel, J. C. Lemonnier, and J. Thomas, J. Phys. F **7**, 2613 (1977).
[54]B. Bartning, Opt. Commun. **4**, 404 (1972); J. Geiger, Z. Naturforsch. **17a**, 696 (1962).
[55]A. R. Krauss and R. Gomer, Phys. Rev. B **13**, 3419 (1976).
[56]H. Boersch, J. Geiger, H. Hellwig, and H. Michel, Z. Phys. **169**, 252 (1962).